Synchrotron light: a success story over six decades

G. Margaritondo
Ecole Polytechnique Fédérale de Lausanne (EPFL)

Abstract

Synchrotron radiation research continues to be a major factor in the progress of science and technology, as it has been for more than one-half century. We present different aspects of its history, starting with an unconventional approach: a fictional version, which should bring to light the reasons that make this field so broadly important. Then, we narrate the real history from three different points of view: the progress of electron accelerators, the evolution of synchrotron-based experiments, and the human factors. Finally, we discuss the present situation, characterized by the arrival of a new generation of sources with exceptional performances: the x-ray free electron lasers (x-FEL's).

E-mail: Giorgio.margaritondo@epfl.ch

I. Foreword[1]

Since its first, timid steps in the 1950's and 1960's, synchrotron research has steadily expanded in size, scope and scientific and technological importance, becoming one of the major cultural enterprises of all times [1-5]. Its present worldwide list of laboratories [6] includes some sixty facilities, with different dimensions and different statuses. Of these, thirteen are free electron lasers -- part of them x-FEL's [7-12].

[1] This review is respectfully and lovingly dedicated to the memory of Francesco (Franco) Cerrina, a most relevant example of the important role of Italian science in this field. Overcoming a difficult personal situation, he obtained his degree at the University of Rome I while working as a technician. After immigrating in the USA, he became a world leader of synchrotron spectroscopy and spectromicroscopy, x-ray optics, synchrotron beamline design, x-ray lithography and microelectronics. He exemplifies the diaspora of too many young Italian scientists in this field (as in many others).

Tens of thousand of users in physics, chemistry, materials science, biomedicine, human heritage, technology and other disciplines exploit these facilities for their research. As the non-proprietary use is typically free of charge, competitive and only based on merit, the synchrotron-FEL network strongly contributes to a culture of equal opportunities for all researchers, overcoming national, financial and gender barriers. And synchrotron experiments produced – and keep producing - many landmark results in science and technology.

What are the causes of this long-lasting and multi-faceted success? Although synchrotron research is complex and extremely diversified, the answer to this question is simple and rooted in basic scientific grounds. To discover it, we will use a rather unusual approach: a fictional tale. The objective of the tale is to reveal the essential factors that make synchrotron radiation so important – but are sometimes difficult to identify within the extreme variety and large mass of activities.

One word of caution is necessary: our fictional and real versions of history are not complete narrations. Indeed, the development of synchrotron research is so voluminous and diversified that a comprehensive account would take a long series of books. We present here a summary, using selected examples of facts and people from this writer's personal experience. The narration, therefore, focuses on facilities that hosted his activities and/or to whose development he contributed: Frascati, the SRC (Synchrotron Radiation Center) in Wisconsin, Elettra in Trieste and SLS (the Swiss Light Source). The corresponding episodes and persons are, obviously, examples of a much wider picture.

Before our fictional account, we would like to host the reader for a short "virtual" visit of a real synchrotron facility [1,2]. Figure 1 shows the panoramic view of the "Sincrotrone Trieste" in Italy. The largest (circular) building houses the Elettra "electron storage ring" operating as a synchrotron source, whereas the long structure on the left contains the FERMI x-FEL facility.

Figure 2 presents simplified schemes of these two kinds of sources. A storage ring (Fig. 2, top) consists of a donut-shaped ultrahigh-vacuum chamber where high-energy electrons are injected and then circulate for a long time (several hours or days) at relativistic speed, under the combined actions of a magnet network and of a radiofrequency system. The main

components of the magnet network are dipole "bending magnets" that deflect the electrons and keep them within closed trajectories. In addition, there are focusing magnets (not shown) and "insertion devices" [13] -- periodic series of magnets installed along otherwise straight parts of the electron trajectory, which cause small transverse oscillations.

The accelerations produced by bending magnets and by insertion devices force the electrically charged electrons to emit electromagnetic waves. These are called "synchrotron radiation" – a rather inappropriate name, as we shall see later. The emission is collected by "beamlines", optically processed along them and delivered to experimental chambers to be used by a variety of instruments.

Due to the emission of synchrotron radiation, the electrons would progressively lose energy and become unable to keep circulating in the ring. The radiofrequency (rf) cavity corrects this problem by periodically restoring the lost energy. This system applies a time-dependent accelerating electric field when the circulating electrons pass through it. Consider a typical storage ring with a ≈500 m perimeter and ≈50 circulating bunches of electrons with speed $\approx c$. A bunch passes through the rf cavity every $\approx(500/c)/50 \approx 3 \times 10^{-8}$ s. Thus, the rf cavity must apply its accelerating field with a frequency $\approx 1/(3 \times 10^{-8}) \approx 3 \times 10^{7}$ Hz – indeed, in the radiofrequency range.

Even with this compensating action, the electrons progressively abandon their closed paths around the ring because of additional phenomena, such as scattering by residual gas particles in the vacuum chamber and the "Touschek effect" [14]. This decreases the emitted radiation, which is proportional to the number of electrons. Additional electrons must therefore be injected.

In the original operation mode, this was done by dumping the residual electron beam and injecting a new one. The present tendency, however, favors a "top-off" mode, in which new electrons are continuously injected. The circulating electron current and the radiation emission are thus kept practically constant for an indefinite period of time.

Figure 2 (top) illustrates one important fact: a storage ring is connected to many experimental chambers – in a real facility, several tens of them. Thus, it simultaneously supports many experiments, strongly decreasing the source-related cost of each of them. In its early days, the

price of synchrotron radiation was less than the publication fees! And a synchrotron facility operates for several decades, prorating over very many experiments the initial construction investments.

We now move our attention to x-FEL's – see the bottom part of Fig. 2. In these sources, electron bunches are periodically injected, accelerated (in most cases by a straight LINAC = "linear accelerator") and used only once to obtain radiation, before being dumped. The emission occurs within a very long insertion device.

We shall discuss later all the details of the x-FEL mechanism. In a nutshell, the interaction between the weakly oscillating electrons within the insertion device and their previously emitted radiation causes a subtle microscopic reshaping of each electron bunch. The new bunch morphology then produces a strong laser-like amplification of the radiation [7-12].

This process enhances the initial spontaneous emission of the electrons, and is called "self amplified spontaneous emission" (SASE) [11]. The most advanced x-FEL's, however, amplify instead "seeding pulses", produced by an external photon source and injected in the system together with the electron bunches. As we shall see, the seeding approach produces x-ray pulses with a better time structure than SASE [7].

The x-FEL geometry can accommodate only a few beamlines (just one is shown in the bottom part of Fig. 2). The source-related cost per experiment is, therefore, higher than for a storage ring. On the other hand, an x-FEL produces ultrashort pulses of exceptional energy. Their peak power is several orders of magnitude larger than for storage rings [7-12], opening the way to entirely new classes of experiments.

All types of synchrotron radiation sources emit radiation with a non-continuous time structure. In a storage ring, the radiofrequency system only acts on electrons that reach it during its accelerating phase. Therefore, the electrons must circulate around the ring in bunches. A beamline is fed with synchrotron radiation only when an electron bunch passes its front-end. Furthermore, each radiation pulse so produced includes many "micropulses" caused by the individual electrons.

In x-FEL's, the electrons accelerated by the LINAC also form bunches that produce photon pulses. The electron bunch length determines the pulse duration, which can be as short as a few femtoseconds, opening the door to very interesting time-dependent experiments.

Note (Figs. 1 and 2) that the typical size of a modern synchrotron or x-FEL facility is gigantic. In the early days, the sources were instead much smaller and with a modest financial support. The birth of this field was not the result of large resources, but of the vision and courage of a small number of pioneers. They bet their careers on the future of synchrotron research, defying the skepticism of colleagues and funding agencies. Our narration is also, if not primarily, a tribute to their bravery.

II. Re-writing History

Our first version of synchrotron history is, as mentioned, a fantasy tale beginning in the 1940's. Quantum mechanics had been introduced four decades earlier and was (almost) universally accepted. Its conceptual foundations were (as still are) rather fuzzy, but the practical successes were astonishing. Quantum notions had been applied to atoms, nuclei, molecules and solids, yielding fundamental theoretical advances.

To profit from them, new experimental techniques and tools were needed. What kinds of tools? To answer, note that the quantum-related properties of solids and molecules are determined by chemical bonds – the common denominator of most scientific and technological activities. Chemical bonds are states of the electrons, and the main interactions affecting electrons are the electromagnetic ones. Thus, the most effective probes to study electrons and chemical bonds are electromagnetic waves, *i.e.*, in quantum terms, photons.

But the situation of photon sources in the 1940's was dismal. Visible sources had been developed for illumination and not for science, and their quality was rather mediocre: lasers were to appear only two decades later. And visible photons were not ideal for analyzing chemical bonds: ultraviolet and x-ray photons would have been much more effective. Indeed, ultraviolet photons have the right energies to explore the valence electrons that directly form chemical bonds. And larger x-ray photon energies can explore core electrons -- which are indirectly affected by the formation of chemical bonds and can yield very valuable information

about them. Finally, x-rays have wavelengths comparable to the chemical bond lengths, and therefore ideal for techniques revealing the atomic structure of molecules and solids.

In the 1940's, however, the ultraviolet and x-ray emitters were even worse than the visible sources. After Wilhelm Roentgen's discovery of x-rays [1], very little progress had been made by their technology.

To understand why, note that the best parameter to measure the quality of a photon source is the "brightness" or "brilliance" b. This parameter is, roughly speaking, proportional to the emitted flux divided by the source size and by the angular spread of the emission. We can understand this definition by considering a laser pointer, which is "good" not only because of its flux but also because of its geometry: the small emitting area and small angular spread concentrate the light in a small spot.

Conventional x-ray sources – based on the electron bombardment of solids - had a low brightness that could not be easily augmented. In fact, the emitted flux could not be strongly increased nor the source size decreased without unmanageable heat dissipation problems. Even the advent of "rotating anodes" [1] did not very much improve this situation.

In our fictional history, research leaders and funding agencies realized the necessity to solve the above problems, because of the potential impact of condensed matter research on the industrial development. And launched in the mid-1940's a big worldwide effort to realize better ultraviolet and x-ray sources. But this enterprise faced a crucial technical obstacle that can be grasped with simple arguments.

The emitted electromagnetic wavelengths roughly scales with the physical dimension of their source. Consider, for example, a solenoid-capacitor circuit LC that emits the wavelength $\lambda = c(LC)^{1/2}/(2\pi)$. For an empty solenoid, L is proportional to $\mu_o A_1 X_1$, where A_1 is the transverse section and X_1 the length. Thus, calling D the LC circuit size, L is not too different from $\mu_o D^2/\mathrm{D} = \mu_o D$. For an empty plane capacitor, $C = \varepsilon_o A_2 X_2$, where A_2 is the surface and X_2 the thickness. Therefore, C is of the order of $\varepsilon_o D^2/\mathrm{D} = \varepsilon_o D$. Overall, λ is not too far from $c(\varepsilon_o\mu_o)^{1/2}D/(2\pi) = D/(2\pi)$, and scales indeed with the source size.

A radio emitter for 1-10 m wavelengths has typical D-values of 0.1-1 m. For x-ray wavelengths of 1 - 10 Å, D should thus scale down to 1 Å or less. In fact, the emitters in a conventional x-ray source are angstrom-size individual atoms. To construct better sources, one would hypothetically require artificial devices, also with angstrom size – impossible to fabricate.

In the fictional tale, clever scientists solved this problem in the late 1940's with an ingenious strategy. They realized that Einstein's relativity offered several ways to virtually "shrink" the source size and the emitted wavelength.

To comprehend how, consider a simple device to emit electromagnetic waves: the dipole magnet illustrated by Fig. 3, with an electron moving at speed v along a circular orbit of radius r in a plane perpendicular to the magnetic field. The centripetal acceleration of magnitude v^2/r causes the emission of synchrotron radiation with the so-called "cyclotron frequency", corresponding to the angular speed ω. Newton's law gives:

$$\frac{m_o v^2}{r} = \text{ Lorentz force magnitude } = evB,$$

and:

$$\omega = \frac{v}{r} = \frac{eB}{m_o}$$

(where e and m_o are the electron charge and rest mass), corresponding to the wavelength:

$$\lambda = \frac{2\pi c}{\omega} = \frac{2\pi c m_o}{eB}.$$

Can this lead to the emission of x-rays? Apparently, not: for example, a field magnitude $B = 1$ tesla gives a ω-value $\approx 1.6 \times 10^{11}$ s^{-1}, corresponding $\lambda \approx 10$ mm, very far from x-rays: a dipole magnet does not seem a good device to produce x-rays.

This negative conclusion, however, is no longer valid if the electron speed is relativistic, $v \approx c$. First, one must consider the Doppler shift, which is a relativistic effect for electromagnetic

waves. The observed wavelength in the laboratory frame R and in the longitudinal direction (that of the electron velocity) is divided by a factor:

$$\frac{\sqrt{1+{}^{v}/_{c}}}{\sqrt{1-{}^{v}/_{c}}}=\frac{1+{}^{v}/_{c}}{\sqrt{1-{}^{v^2}/_{c^2}}}\approx 2\gamma,$$

where γ is the electron energy divided by the rest energy $m_0c^2 \approx 0.5$ MeV.

The Doppler effect thus moves the emission towards smaller wavelengths. And another relativistic phenomenon works in the same direction: let us discover it.

Consider the inertial reference frame R' whose velocity instantaneously coincides with that of the electron. Note that this is *not* the frame of the electron, which is accelerated and therefore not inertial. In R', the electron emits radiation because it has zero velocity but not zero acceleration. What is the force causing this acceleration? Since the electron speed in R' is zero, the Lorentz force disappears. But the relativistic transformation of the electromagnetic field gives in R' not only a B-field but also an electric field in the plane of the orbit, with strength $E = \gamma vB$. Thus, the force in R' is electrostatic and of magnitude γevB, and the cyclotron frequency becomes:

$$\omega' = \gamma\frac{eB}{m_o}.$$

The corresponding emitted wavelength is:

$$\lambda' = \frac{2\pi c}{\omega'} = \frac{1}{\gamma}\frac{2\pi c m_o}{eB}.$$

Combined with the Doppler shift, this gives in the R-frame the wavelength:

$$\lambda \approx \frac{\lambda'}{2\gamma} = \frac{1}{2\gamma^2}\frac{2\pi c m_o}{eB}.$$

i.e., the classical value divided by $2\gamma^2$.

Consider, for example, an electron energy of 1 GeV, corresponding to $\gamma \approx 2{,}000$ and to $2\gamma^2 \approx 8 \times 10^6$. A millimeter-size emitted wavelength in the classical case would relativistically dwindle to $\approx 0.001/(8 \times 10^6) \approx 1.2$ Å. Voilà: relativity takes the large-sized dipole magnet of Fig. 3 and shrinks its emitted wavelength to x-ray magnitudes!

A similar result is obtained for the emission of the insertion device schematically shown in Fig. 4 -- called "undulator" and consisting of a regular series of magnets with period H. Consider an electron with a relativistic longitudinal speed $v \approx c$ in the laboratory R-frame (Fig. 4, top). Seen in the inertial R'-frame that moves with the same longitudinal speed v, the period H is shortened to H/γ by the Lorentz contraction (Fig. 4, middle). Furthermore, the Lorentz transformation of the periodic B-field gives in the R'-frame transverse magnetic and electric fields with equal periods and perpendicular to each other, both traveling at a speed $-v \approx -c$. In other words, the electron "sees" the undulator as a pseudo-electromagnetic wave with a short wavelength H/γ.

The interaction between this pseudo-wave and the electron produces a backscattered wave: this is the cause of synchrotron radiation. The emitted wavelength is H/γ in the R'-frame. But, in the laboratory R-frame (Fig. 4, bottom), the Doppler effect divides it by $\approx 2\gamma$, giving $\lambda \approx H/(2\gamma^2)$. Note the $2\gamma^2$ factor, the same as for dipole magnets!

The two special cases discussed above can be generalized. Any device emitting synchrotron radiation must have at least one electric charge with an accelerated transverse motion. The detected radiation depends not only on this transverse motion, but also on the longitudinal motion.

The transverse motion is caused by the magnetic field of a device, *e.g.*, an undulator or a bending magnet. To analyze the phenomenon, one must first accurately define the reference frames. The laboratory frame R is of course that of the device and of the observer. The definition of the "electron" R'-frame is trickier, as we already saw: it is not the non-inertial frame of the accelerated electron but the inertial frame moving with the same instantaneous longitudinal velocity as the electron.

The electromagnetic field transformation from R to R' has two effects: first, it adds an electric field to the magnetic field. Second, it Lorentz-contracts the longitudinal device size, dividing it by γ. The same factor applies to the emitted wavelengths in R'. And, when detected in R, the wavelengths are Doppler-shifted by a factor $\approx 2\gamma$ in the longitudinal direction.

Hence, the wavelengths are divided by a factor $\approx(\gamma)(2\gamma) = 2\gamma^2$ with respect to the non-relativistic case. The relativistic longitudinal motion thus shortens the wavelengths by many orders of magnitude, reaching x-ray levels even when the non-relativistic emission would have occurred in the radiofrequency range.

For undulators, a typical magnitude of H is 0.01 m, so the central wavelength $\approx H/(2\gamma^2)$ can reach angstrom-level x-ray values if γ is of the order of 10^4, *i.e.*, if the electron accelerator has an energy or several GeV's. In our fictional history, after realizing this fact the funding agencies quickly and generously provided large financial resources to build such accelerators. We can imagine that their this effort would have taken approximately one decade, from the late-1940s to the late-1950's, producing at first the pulsed accelerators called "synchrotrons".

These machines inspired the name "synchrotron radiation". But, a few years later, better accelerators started to be used as radiation sources: the "storage rings" -- in which relativistic electrons circulate for days continuously emitting electromagnetic waves. The technically obsolete name "synchrotron radiation" continued nevertheless to be universally used.

The first tests of storage rings for synchrotron radiation applications produced excellent results. This stimulated further, massive investments: we can fantasize that a worldwide network of synchrotron radiation facilities became available in the 1960's [6].

The brightness of storage ring sources grew steadily. To understand how, we must consider again the three factors that produce high brightness: a small angular divergence of the emission, a small source size and a large flux.

The angular collimation is another product of relativity. As illustrated by Fig. 5 (bottom), the longitudinal electron motion "projects" in the forward direction the emitted radiation (in this

case from of an insertion device). This is similar to what occurs everyday for non-relativistic wave emitters like the klaxon of a car (Fig. 5, top). But relativity makes it extreme.

The reason is that the Lorentz transformation of the photon velocities from R' to R divides the transverse components by γ, but not the longitudinal components. Consequently, the photon velocities are confined to a very small angular range $\approx 1/\gamma$ around the longitudinal direction.

The second factor producing high brightness is a large flux. In a synchrotron source, boosting the flux is possible since the emitting electrons are in vacuum and not in a solid, hence largely immune from heat dissipation problems.

Furthermore, the emitted flux is strongly enhanced by relativity. Consider for example the dipole magnet of Fig. 3: in the non-relativistic limit, the total emitted power P is proportional to the square a^2 of the (transverse) acceleration, according to Larmor's equation:

$$P = \frac{2}{3}\frac{e^2}{4\pi\varepsilon_o c^3}a^2.$$

This, however, is only true for electron speeds much smaller than c; in particular, it works in the above-defined R'-frame, where the instantaneous speed is zero:

$$P' = \frac{2}{3}\frac{e^2}{4\pi\varepsilon_o c^3}a'^2.$$

To calculate the corresponding emitted power P in the R-frame, we must Lorentz-transform the emitted energy and the time. Calling Ω and Ω' the emitted energies in the two frames and t and t' the times, we have:

$$P = \frac{d\Omega}{dt} = \frac{d\Omega}{d\Omega'}\frac{d\Omega'}{dt'}\frac{dt'}{dt} = \frac{d(\gamma\Omega')}{d\Omega'}\frac{d\Omega'}{dt'}\frac{dt'}{d(\gamma t')} = \frac{d\Omega'}{dt'} = P'.$$

Thus, the emitted power is Lorentz-invariant, and the above Larmor value expressed in terms of a' in the R'-frame is also valid for the R-frame.

To express P in terms of the acceleration a in R, we must Lorentz-transform a'. The accelerations are the second time derivatives of the transverse positions, which are Lorentz-invariant. Thus, the Lorentz transformation of time gives $a' = \gamma^2 a$. In summary:

$$P = P' = \frac{2}{3}\frac{e^2}{4\pi\varepsilon_o c^3}a'^2 = \gamma^4\frac{2}{3}\frac{e^2}{4\pi\varepsilon_o c^3}a^2.$$

In summary, relativity multiplies the classic Larmor emitted power by γ^4. This is a key discovery, since the γ^4 factor is huge, thus relativity boosts both the flux and the brightness.

The above result can be expressed in a slightly different way, using the radius r of the electron orbit in the dipole magnet. The acceleration a equals $v^2/r \approx c^2/r$, so:

$$P \approx \gamma^4\frac{2}{3}\frac{e^2 c}{4\pi\varepsilon_o r^2},$$

a simple equation whose numerical evaluations show how large is the emitted synchrotron radiation power. And this is only the emission of a single electron, whereas in a storage ring there are many circulating and emitting electrons.

The third factor giving high brightness is a small source size, i.e., a small transverse cross section of the electron beam. There is a conflict between the mission of synchrotron sources – emitting radiation – and the need for a small source size. In fact, the photon emission is a stochastic process that changes by different amounts the energies of different circulating electrons. Different energies correspond to slightly different trajectories, and this increases the electron beam cross-section. In accelerator-physics jargon, the radiation emission "warms up" the electron beam.

This problem can be removed by using the electron beam only once, with no previous history of radiation emission: this is what happens in a LINAC. But using an accelerated electron beam only once is expensive -- whereas in a storage ring the beam produces radiation for days. The higher cost can only be justified by exceptional characteristics of the emission: this is, as we shall see, the case of x-FEL's.

For storage rings, there is no easy solution: the source size must be limited by a sophisticated electron beam control system. Fortunately, accelerator science made fantastic progress in improving this technical performance.

In our fictional narration, by the late 1950's storage rings could to deliver all three factors required for high brightness: strong angular collimation, high emitted power and small source size. Such characteristics are reminiscent of those of a laser -- but a standard (storage ring) synchrotron source is *not* a laser.

Constructing real x-ray lasers was nevertheless very desirable: they would have produced photon pulses with exceptionally high power and brightness. This goal was realized with a novel technology beyond that of storage rings: the x-FEL's.

Figure 6 (top) schematically explains the details of the x-FEL mechanism [7-12]. A bunch of relativistic electrons travels towards an undulator. After entering the undulator, the electrons emit synchrotron radiation waves that, subsequently, travel together with them along the undulator axis. The (transverse) magnetic field of the wave, combined with the transverse velocity of the undulator-induced electron oscillations, produces Lorentz forces that "push" the electrons in the longitudinal direction.

This slightly modifies the position of each electron within its bunch -- reshaping the bunch structure by concentrating the electrons within periodic "slices", with period equal to the wavelength. Afterwards, the emissions from electrons in these "slices" constructively interfere with each other, amplifying the initial wave. This "optical amplification" is somewhat reminiscent of a conventional laser, but the two mechanisms are fundamentally different.

Why does the slice periodicity correspond to one wavelength? The bottom part of Fig. 6 explains this point. The wave magnetic field $\boldsymbol{B}_{\mathrm{w}}$ (green) and the transverse electron velocity $\boldsymbol{v}_{\mathrm{T}}$ (blue) cause the Lorentz forces (red). These slightly shift the positions of the electrons along the bunch until they reach one of the wave nodes. Taking into account all the vector directions, the slices are created at every other node, so their spacing equals one wavelength.

Note that after one-half transverse electron oscillation the direction of $\boldsymbol{v}_{\mathbf{T}}$ changes but those of the Lorentz forces do not. This is due to the small speed difference between the electrons and the wave – see [7] for details.

The practical implementation of the FEL mechanism must be accurate enough to avoid the destruction of the delicate bunch microstructure. The mechanism can work both for x-rays and for larger-wavelength infrared radiation. In practice, though, infrared FEL's were realized several decades before x-FEL's: why?

The creation of "slices" might actually seem more difficult for an infrared FEL than for an x-FEL: the wavelength is longer and so is the slice periodicity -- necessitating larger electron displacements. But this is not the entire story: the emission of x-rays requires large γ-values. And this strongly increases (by a factor γ^3) the electron "longitudinal relativistic mass" [7] (a theoretically questionable but practically useful notion). So, whereas the bunch reshaping in an x-FEL requires small displacements, it must be achieved by "pushing" very heavy electrons -- and this last factor outweighs the first.

Furthermore, the bunch microstructure of an x-FEL, consisting of slices very close to each other, can be easily destroyed. Its preservation requires very accurate instrumentation to avoid fatal perturbations.

Finally, a problem affects all kinds of x-ray lasers: the lack of optical cavities. In a visible or infrared laser, an optical cavity consisting of two parallel reflecting surfaces practically extends the photon path and enhances the optical amplification. But this is not possible for x-rays, since the normal-angle reflectivity is very weak. Thus, the amplification must yield the desired emission within a single pass.

All these different difficulties slowed down the implementation of x-FEL's. In our fictional account, infrared FEL's were realized shortly after storage rings, in the late-1950's, whereas x-FEL's arrived four decades later. But the final results were fantastic: the peak brightness of x-FEL's was exceptionally high and their pulses exceedingly short. This opened the way to previously unimaginable experiments.

All along our fictional tale, synchrotron radiation stimulated advances in accelerator technology that also profited elementary particle physics. But the two developments were not equivalent, since particle physics also required hadron accelerators that are totally unsuitable for synchrotron radiation. We have seen, indeed, that the emitted power for a dipole magnet is proportional to γ^4, and therefore to $1/m_o{}^4$. This effectively kills the synchrotron emission of hadrons. A similar conclusion is valid for other synchrotron radiation sources.

What can we learn from the fictional tale? First, the development of synchrotron radiation could have been much faster. If condensed matter research had been the priority, then each generation of synchrotron radiation facilities would have been anticipated by one or two decades. But the real history was different: elementary particles dominated the development of accelerators. We may find this regrettable, but must honestly recognize that the colleagues in elementary particle research merited the priority with their visionary strategies.

The fictional tale also taught us that the needs of chemical bond research, ubiquitous in modern science and technology, could only be met by exploiting relativity with sophisticated electron accelerators. Synchrotron radiation constitutes indeed the most important practical application of relativity.

Incidentally, it also provides an opportunity to "watch" relativity in action. In some facilities, visible synchrotron radiation can be observed through special windows. And this visible light is the tangible evidence of two relativistic effects: Lorentz contraction and Doppler shift.

III. The Real History, on the Accelerator Side

Accelerator technology for elementary particle studies also paved the way to the development of synchrotron radiation [15-22]. But, initially, the emission of x-rays came into the picture only indirectly. The accelerators called "betatrons" were designed in the 1930's to accelerate the electrons ("beta particles") and hit solid targets to emit x-rays – not for condensed matter research but for nuclear experiments, oncology and other applications [23].

Furthermore, the initial interest in synchrotron radiation was not stimulated by its potential use, but by its impact on the operation of lepton accelerators: it notably limited the energy of

betatrons. This motivated in the 1930's and 1940's the formulation of theories of synchrotron emission by Dimitri Ivanenko, Isaac Pomeranchuk and coworkers in the Soviet Union [24] and by Julian Schwinger in the USA [25]. But their formalism was very complicated, so the results remained essentially unknown outside a small circle of accelerator scientists.

Further complicating the picture, the first betatrons had energies of only 0.01-0.1 GeV, thus their synchrotron radiation wavelengths were limited to the visible and infrared ranges. Interestingly, the initial search for the emitted radiation in the 1940's, at the General Electrics (GE) Laboratory in Schenectady [16], failed because the detectors were not even for visible light but for radio waves and microwaves – the expected emission if relativity was not taken into account.

The observation of synchrotron radiation [16] had to wait until 1947 and was accidentally achieved with one of the first synchrotrons, a 0.07 GeV machine also at GE [23]. Synchrotrons were the successors of the so-called "cyclotrons", machines in which charged particles were progressively accelerated while traveling along a spiral-like trajectory under the combined influence of a constant magnetic field and of a periodic electric field. The spiral path required a large vacuum chamber and complicated the entire operation: a closed orbit was more desirable. Furthermore, as the particle speed increased so did the mass, and the classical version of a cyclotron no longer worked. To solve these problems, Vladimir Veksler and Edwin McMillan [26] independently conceived the strategy of increasing the magnetic field strength synchronously with the growth of the particle energy – inspiring the name "synchrotron".

At GE, Frank Elder, Anatole Gurewitsch, Robert Langmuir and Herb Pollock [16] observed a mysterious visible light in their synchrotron and quickly recognized its nature as synchrotron radiation (Fig. 7). This was by no means a trivial achievement: without relativity, one would expect millimeter or centimeter wavelengths -- not visible light. The real properties could only be understood after penetrating the heavy formalism of synchrotron emission theories.

The notion of practically using the emission was even less evident. But an idea slowly emerged: by increasing the electron energy, one could extend the spectrum to ultraviolet light and x-rays – spectral domains for which the sources were notoriously scarce and

heartbreakingly bad. Diran Tomboulian and Paul Hartman successfully tested this notion in 1956, with the 300 MeV synchrotron of Cornell University.

But it was only in 1961 that Robert Madden and Keith Coddling started the first synchrotron radiation experimental program [28]. These visionary pioneers used the 180 MeV electron synchrotron "SURF" of the National Bureau of Standards (NBS, what later became NIST, the National Institute of Standards and Technology). Why was NBS interested in synchrotron radiation? Its spectral properties could be accurately calculated from theory, so it provided a calibration standard for ultraviolet detectors. And the use of ultraviolet rays was expected to expand -- for example, to preserve milk and sliced salami in supermarkets…

Shortly afterwards, a few other pioneers initiated spectroscopy experiments at Frascati [17], INS-SOR in Tokyo, DESY in Hamburg and Daresbury. These rather heroic efforts – notably by Yvette Cachois *et al.* in Frascati [29] using the 1.1 GeV machine (Fig. 8) built under the direction of Giorgio Salvini - confirmed the potential of synchrotron radiation for condensed matter research. And the characterization of the emission validated the theoretical predictions.

But, in practical terms, synchrotron radiation research using real synchrotrons was going nowhere, because of a critical problem. Each electron bunch circulated only once around the synchrotron before being dumped, and new bunches had to be continuously injected. This produced intense, dangerous radiation and strong pulses in the experimental electronics. The life of the early users was utterly miserable (as this writer, alas, personally experienced).

For example, the dangerous radiation forced scientists to stay outside the radiation-shielded area surrounding the synchrotron whenever it was in operation – typically, for many hours. Simple operations like a sample alignment - which today take a few minutes - were performed in steps separated by hours, taking a week or more!

Only a few visionaries accepted to work under such difficult conditions. I would like to mention the pioneers of the first sustained synchrotron radiation program in Frascati, led by Gianfranco Chiarotti and including, in particular, Adalberto (Camillo) Balzarotti, Mario Piacentini, Emilio Burattini, Antonio Bianconi and Martino Grandolfo [30,31].

Fortunately, in the mid-1960's a new development in accelerator technology revolutionized synchrotron research. Continuous storage rings came into the scene [14,17], replacing the pulsed operation of synchrotrons. The users could work close to the source without long time breaks, and the emission could be considered, for most applications, practically time-independent.

Two institutions were particularly well placed to lead this revolution: the University of Wisconsin and the Frascati National Laboratory. In both cases, their advantage was the result of circumstances not related to synchrotron radiation.

At the University of Wisconsin-Madison, Tantalus (Fig. 9), a prototype 240 MeV storage ring with a 9.38 m circumference, had been constructed in the late 1960's under the leadership of Ednor M. (Ed) Rowe (Fig. 10) and Fred Mills [19-23]. This was the end product of a consortium of universities, MURA (Midwest Universities Research Association), whose scope was to attract to its region a national accelerator laboratory [23] (what later became Fermilab).

MURA developed Tantalus to prove its technical capabilities. But it was nearing dissolution in 1967 without attracting a large facility. So, there was no money to complete the prototype and no mission for it -- a situation that inspired the tantalizing name "Tantalus".

But a group of extraordinarily illuminated scientists, including Ed Rowe himself, Fred Brown, David Lynch and Helmut Fritzsche, conceived a new idea: why not use Tantalus as a full-time, dedicated synchrotron source [18-22]? This notion, revolutionary beyond belief, was widely greeted with skepticism: how in heaven could one find the four or five user groups needed to justify investing good money in a *dedicated* synchrotron source? Only with reluctance, some funding agencies finally (and barely) granted the money to test it.

But the test succeeded: the first synchrotron radiation experiment with a dedicated source was performed (Fig. 11) on Tantalus by Ulrich Gerhardt and coworkers of the team of Helmut Fritzsche, at 10:40 a.m. of August 7, 1968. This was the real birth of modern synchrotron research as well as of the Wisconsin Synchrotron Radiation Center (SRC) [18-22].

With all the advantages of a storage ring and of a dedicated facility, SRC attracted in the following years scientists from all over the world. It was the testing ground for a large portion of the modern synchrotron research techniques, the factory of many of the experimental results of that period and a training ground for future leaders and managers in synchrotron radiation – such as Patrick Soukiassian, Wolfgang Eberhardt, Niels Mårtensson, Ernst Koch and Bruno Reihl,.

SRC evolved with time: in 1986, it inaugurated Aladdin, a new 1 GeV storage ring. In spite of very limited resources compared to other synchrotron facilities, it continued its international role until its untimely shutdown in 2014 (arguably, one of the worst decisions ever made by the US National Science Foundation).

In Frascati, the activity [14,32] on storage rings had started in the early 1960's under the leadership of Carlo Bernardini and Bruno Touschek (Fig. 12) (an outstanding Austrian physicist of Jewish descent on the mother side, who had miraculously escaped being murdered by a Nazi in 1945 [33]). They directed a top-class team, including the future x-FEL father Claudio Pellegrini. The first Frascati storage ring was a miniature prototype baptized "AdA", from "*Anello di Accumulazione*"("storage ring"). But there was a rumor that the real inspiration was Touschek's aunt Ada.

The success of the prototype paved the way to the first collider storage ring Adone ("big Ada"), reaching the energy of 1.5 GeV per beam – see Fig. 12. Commissioned in 1967, Adone was a superb machine, putting Frascati at the forefront of storage ring technologies. Its elementary particle research output was also quite good. But, regrettably, Adone missed the main high-energy discovery of its time, the J/Ψ particle. This was mere misfortune: the J/Ψ energy was only 0.05 GeV beyond its range. Reconfigured in a few hours, it confirmed the discovery within days and opened the door to two Nobel prizes – alas, not in Frascati [34].

Adone was also an excellent source of synchrotron radiation. A new program was launched in 1976 [34] to exploit its emission: PULS (Progetto di Utilizzazione della luce di Sincrotrone, Project for the Use of Synchrotron Light), headed by Franco Bassani (Fig. 13, left). PULS produced good science and trained several Italian scientists who later became synchrotron radiation leaders, notably Franco Cerrina (Fig. 13, right), Paolo Perfetti and Francesco Sette.

In this writer's opinion, however, Adone did not reach its full potential as a synchrotron radiation facility because it never became a fully dedicated source like Tantalus. And it was not supported with resources comparable to the new facilities that were being commissioned in Hamburg, Brookhaven and elsewhere. Frascati could have become the world leader in synchrotron radiation thanks to an extraordinary combination of very advanced technical know-how and talented young scientists. But Adone remained instead a shared machine and was dismantled in 1993 – so that many of the Frascati synchrotron scientists left Italy for other countries.

In the meantime, the interest in synchrotron radiation had ballooned: dedicated sources had become the norm. The facilities of this "second generation", mostly commissioned in the early 1980's, included SRS at the Daresbury Laboratory in the UK, NSLS at the Brookhaven National Laboratory, Aladdin in Wisconsin, the Photon Factory at the KEK laboratory in Tsukuba, BESSY in Berlin, SuperACO at LURE (Orsay). Furthermore, some previously shared-use machines became dedicated sources, notably SSRL at SLAC, Stanford, HASYLAB at DESY in Hamburg and, progressively, CHESS at Cornell University.

The next step, the "third generation" of synchrotron sources, was triggered by the conceptual evolution in the assessment of the source quality. Until the 1980's, the main objective was to increase the emitted flux. But the focus gradually shifted to the brightness, taking also into account the emission geometry. The reason was quite fundamental [1]: one version of the phase-space-volume conservation Liouville theorem states that the brightness is conserved along a (lossless) beamline. This implies that a source with high brightness facilitates the task of delivering many photons per second into a small sample area (for example, for microscopy).

Before this conceptual evolution, synchrotron radiation was almost exclusively extracted from the "bending magnets" of the accelerator network -- which had the simultaneous mission to keep the electron beam in a closed trajectory. Bending magnets did produce intense radiation, but their dual mission limited the flexibility in optimizing them as synchrotron sources. And the brightness was also limited, for example because the horizontal angular spread was the entire angle corresponding to the entrance of each beamline.

As the focus shifted from flux to brightness, insertion devices were increasingly used as sources to overcome the limitations of bending magnets. These included the aforementioned "undulators" and the so-called "wigglers" [13].

What is the difference between undulators and wigglers? Both classes of devices are periodic magnetic fields as seen in Fig. 4, but the wigglers have stronger magnetic fields. This causes basic differences in their emissions [1,13].

As illustrated in Fig. 14, the stronger magnetic field of a wiggler produces larger electron transverse oscillations than an undulator. Due to the narrow angular spread of the emission cone, each electron passing through a wiggler delivers a series of short synchrotron radiation pulses to a (point-like) detector. Each pulse is similar to the emission detected when an electron passes through a bending magnet, but the total energy of the pulse series is larger.

An undulator, which only produces weak transverse oscillations, causes a single, longer pulse at the detector instead of a pulse series. Due to the properties of the Fourier transforms, the corresponding frequency (or wavelength) bandwidth is narrower than for bending magnets or wigglers. Hence, the radiated energy is concentrated within a small spectral region.

In 1981, Klaus Hallbach (Fig. 15), Kwang-Je Kim and co-workers [13] of the Lawrence Berkeley Laboratory demonstrated at SSRL the first use of an insertion device as a synchrotron source, under the leadership of Dave Attwood. Motivated by this success, several institutions contributed to the evolution of undulators and wigglers throughout the 1980's, notably the outstanding Budker Institute team in Novosibirsk, led by Gennady Kulipanov.

The focus on brightness also led to new designs of storage rings. The geometry of the "third generation" facilities included long straight sections to accommodate insertion devices. And their magnet system further enhanced the brightness, notably using the Chasman-Green double-bend achromat lattice principles [15] to decrease the "emittance" (the combination of source size and angular divergence). Many sources of this class were commissioned over the world, for example Elettra in Trieste (Fig. 1), the Swiss Light Source (SLS, Fig. 16), Max-lab in Sweden, ALS in Berkeley, APS in Argonne, ESRF in Grenoble Spring-8 in Japan, SRRC in Taiwan and the Pohang source in Korea.

Elettra was particularly important for Italian scientists, since it compensated to a good extent the strategic mistake of the non-dedicated use of Adone. The project was conceived and implemented under the leadership of the Nobel laureate Carlo Rubbia. Its first accelerator director, Mario Puglisi, represented an historical link with the original Adone team. After Puglisi's premature death (a few weeks before commissioning Elettra), the project was timely completed under the direction of another outstanding accelerator scientists, Albin Wrulich. And the launching of the facility could count on research leaders like Renzo Rosei, Luciano Fonda, Carlo Rizzuto, Giovanni Comelli, and later Massimo Altarelli and Alfonso Franciosi. And on a remarkable experimental team including Maya Kiskinova, Michele Bertolo, Giorgio Paolucci, Adolfo Savoia, Giuliana Tromba, Kevin Prince, Fulvio Parmigiani and others.

The "revenge" of Italian synchrotron scientist was not limited to Elettra. One should note their key role at ESRF, with leaders like Massimo Altarelli, Francesco Sette, Settimio Mobilio and Federico Boscherini, as well as the use of the new Frascati accelerator DAFNE, notably by Antonella Balerna.

In parallel to the accelerator progress, the focus on brightness stimulated the technical evolution of monochromators and photon detection systems. Monochromators were particularly important, since most synchrotron applications require a very narrow band of wavelengths. We have seen (e.g., Fig. 14) that the wavelength bandwidth of wigglers and bending magnets is very broad. The bandwidth of undulators, although narrower, is still too large for most applications and requires further spectral filtering.

Monochromators do extract narrow wavelength bands from the broadband emission of bending magnets and wigglers. Over the years, their technological evolution produced excellent instruments with famous names like Seya-Namioka, Grasshopper, ERG (extended range grasshopper), TGM (toroidal grating monochromator) and Dragon.

The extraction of narrow wavelength bands from undulators is more complicated. In addition to monochromator filtering, it also requires changing the central wavelength of the emission: let us see how [1]. The central wavelength $\lambda \approx H/(2\gamma^2)$ depends on the γ-factor. But what exactly is this factor? In reality, it corresponds to the energy of the *longitudinal* electron motion, which determines both the Lorentz contraction and the Doppler shift.

The transverse oscillations induced by the undulator decrease the energy of the longitudinal motion, since the Lorentz force does not do any work and therefore cannot change the total kinetic energy. This decrease depends on the amplitude of the transverse oscillations, which increases with the B-field strength. Thus, by changing the B-field (for example by modifying the magnets gaps), one can change the central emitted wavelength.

Incidentally, the theory of synchrotron radiation explains in detail the emission spectra of each class of sources [2,4,24,25]. But the essential facts can be grasped with simple arguments. Consider for example bending magnets: we have seen that the emission is centered at the wavelength:

$$\lambda \approx \frac{1}{2\gamma^2}\frac{2\pi c m_o}{eB}.$$

The bandwidth $\Delta\lambda$ around this peak can be derived [1] using the Fourier transforms, from the duration Δt of the photon pulse produced by an electron passing through the magnet, obtaining $\Delta\lambda \approx \lambda/2$. In first approximation, one can thus imagine the bending magnet spectrum as a broad peak. This is close to the real spectrum, although the conventional log-log plot may conceal its nature.

With the progress of monochromators, particle detectors and other optical components, matched the progress of the sources, the overall beamline design became more sophisticated. The main instrument was the "Shadow" software (Fig. 17), which transformed the "art" of developing beamlines into an advanced and flexible engineering task. The leader of the "Shadow" development was Franco Cerrina at Wisconsin, who made it the world standard for beamline design [35].

The final chapter of the accelerator-related synchrotron radiation history is still underway: the advent of x-FEL's. Their technical aspects were already discussed and their use will be treated in detail in Section V. Here, we will remark (Fig. 18) their contribution to the historical growth of x-ray brightness.

This progress has been objectively spectacular over many decades. It consistently outpaced other technological achievements that enjoy wider popularity -- such as the power and

storage capacity of supercomputers or the spatial resolution of electron microscopy. This poses a constant challenge to synchrotron radiation users, pressed to adequately exploit such exceptional facilities - and makes their professional lives demanding but also very exciting.

IV. The Experiment Side

The development of synchrotron radiation research was marked by a continuous cross-fertilization between instrumentation and experiments. The types of studies kept changing, primarily because of the evolving scientific interests.

As an example, consider the synchrotron spectroscopy studies of superconductivity [36,37]. In the first two decades of synchrotron research, superconductivity was out of its reach. The reason was the energy scale of conventional superconductors, related to the width 2Δ of the superconducting gap – which increases with the critical temperature. For conventional superconductors, 2Δ is of the order of meV's, thus far smaller than the resolution of synchrotron spectroscopies of that time.

The discovery in 1986 of high-temperature superconductivity suddenly brought the energy scale within the reach of synchrotron photoemission spectroscopy. This stimulated instrumentation advances that bridged the remaining difference [36]. And opened the door to a variety of experiments, not only about the gap itself but also on other important aspects like the spatial symmetry of the superconducting state [38]. Superconductivity thus became a leading subdomain of synchrotron research.

For a more general picture of the interplay between experimental interests and synchrotron radiation techniques, we shall consider five main classes of applications [1]: (1) spectroscopy; (2) structural techniques; (3) x-ray imaging; (4) microscopy and spectromicroscopy; (5) applied technologies. Among these, photoemission spectroscopy caused in the 1970's the first revolutionary impact of synchrotron radiation on condensed matter research: let us see why.

IV.1. Photoemission

In the early years of synchrotron research, ultraviolet absorption and reflection spectroscopy played a dominant role. The reasons were practical as well as conceptual. The first dedicated synchrotron sources did not have sufficient energy to deliver the short wavelengths required for structural or core-level analysis. And they did not produce sufficient intensity and brightness for other spectroscopies (or microscopies) besides absorption/reflection techniques. Furthermore, many of the initial synchrotron users were condensed-matter physicists, and absorption/reflection spectroscopy was very prominent in their discipline during that historical period.

The first dedicated source Tantalus provides an excellent example of that phase. Its initial electron beam current (<1 mA) produced a weak emission not allowing much more than ultraviolet absorption measurements. This changed in the 1970's, when a new electron injection system brought the current to several mA's (and later >100 mA): the emitted intensity became sufficient for photoemission, which looked like a very exciting type of spectroscopy [1,39-41].

The conceptual reasons are simple: the photoelectric effect connects the measurable features of free electrons in vacuum with those of electrons inside solids and molecules – which cause most of the condensed-matter properties. The connection was first established by the revolutionary Einstein's hypothesis [42] on the existence of photons, and by his consequent prediction of the photoelectron properties. For example, the energy distribution of the photoelectrons in vacuum primarily mirrors that of the electrons in the analyzed system, shifted upwards by the photon energy.

Einstein's theory implied that photoemission could verify the predictions of quantum mechanics about solid and molecules, and discover new properties. However, the realization of this opportunity faced two formidable obstacles that delayed it by one-half century. First, the "escape depth" of photoelectrons from a solid, caused by inelastic scatterings, is so short (a few angstroms) that their properties are heavily affected by the surface and its contamination. This problem was eventually eliminated by ultrahigh-vacuum technology, which could preserve clean surfaces for the duration of a photoemission experiment.

The second problem was caused by the technical limitations of pre-synchrotron sources of ultraviolet and x-ray photons. Not only their emission was weak, but most of them only

produced one wavelength. This sharply restricted the information extractable with photoemission techniques.

Storage-ring synchrotron sources dramatically changed this situation. For example, one could explore the effects of the photon energy on the photoemission process. Previously, a typical photoemission experiment measured the energy distribution of the ejected photoelectrons while bombarding the specimen with one single photon energy – see Fig. 19a. The energy distribution curves (EDC's) of the photoelectrons were then used to derive the original energy distribution of electrons inside the specimen.

However, as the photon energy remained constant, different initial states of the process corresponded to different final states. Thus, the EDC's were also affected by the changes in the transition probability. Disentangling the desired information – the initial-state energy distribution - from these "matrix element effects" was not trivial.

With synchrotron sources, one could perform photoemission experiments at different photon energies, identifying the transition probability effects. This was demonstrated, notably, by Dean Eastman's IBM team [43] (which over the years trained many future world leaders of synchrotron radiation like John Freeouf, Wolfgang Gudat, Ward Plummer, Tai Chiang, Jim Knapp and Franz Himpsel).

With the variable photon energy one could also implement entirely new photoemission techniques. Such as the constant-initial-state (CIS) and constant-final-state (CFS) spectroscopies invented by Jerry Lapeyre – see Fig. 19a [44,45]. In the CIS mode, the photon energy and the collected photoelectron energy (the "final state" energy) are simultaneously scanned while keeping constant their difference, equal to the initial-state energy. The corresponding spectra reflect the density of unoccupied (final) states, complementing the information on occupied states from the EDC's – see Fig. 19b [46].

In the CFS mode (see Fig. 19a and the example of Fig. 19c), the photoemission intensity is measured at a constant energy while scanning the photon energy. The spectra reflect the density of occupied states like the EDC's. However, by keeping constant the final-state energy one strongly reduces the "matrix element effects".

A variant of the CSF mode was the "(partial) yield spectroscopy" invented by Ruprecht Haensel *et al.* [46] and by Wolfgang Gudat and Christof Kunz [48] – see the example of Fig. 20 [49]. In this case, the constant photoelectron energy is very low, so that one primarily detects "secondary" photoelectrons, which lost part of their energy after the initial optical excitation and before exiting the sample. As a result, the partial-yield spectra are simply proportional to the photon absorption coefficient. However, because of the short photoelectron escape depth, the measured absorption coefficient is not that of the bulk sample but of its surface. These spectra carry very valuable information on phenomena like chemisorption and catalysis.

Synchrotron radiation was also a primary factor in the developments in photoemission with angular resolution. The high intensity produced indeed large signal levels even when the photoelectron detection was limited to a narrow angular range. Synchrotron sources also allowed measuring photoemission spectra for different photon polarizations and, in later years, for different spin polarizations. All the above developments sharply increased the amount and quality of the information provided by the different photoemission techniques [39-41].

Figures 21 and 22 show examples of early angle-resolved photoemission results, produced at Tantalus. In Fig. 21, we see the directional dependence of the photoemission intensity corresponding to the d-electrons of the layer compound 1T-TaS_2. The angular variations clearly reflect the symmetry of the photoemitting crystal. Such spectacular results, obtained by Mort Traum and Neville Smith in collaboration with Jerry Lapeyre's team [50], had a strong historical role. Indeed, they eradicated earlier, wrong ideas: many authors expected the directional effects in photoemission to be wiped out by elastic scatterings before the exit from the sample.

The consequence was a huge number of applications of "ARPES" (Angle-Resolved Photoemission Spectroscopy). In essence, ARPES broadened the objectives of photoemission, from the mere energy distributions of the electrons to their k-vectors. The k-vectors of the photoelectrons were derived from their energy and direction of motion. Then, one could retrieve the initial k-vectors of the electrons in the specimen. This yielded, in particular, the energy *vs.* k curves -- *i.e.*, the band structure in the case of crystalline solids. Figure 22 shows an early example of experimental band mapping [51].

Connecting the photoelectron k-vectors to those of electrons inside the specimen was not trivial, since they changed as the particles crossed the surface. The initial tests of experimental band mapping concerned two-dimensional layered crystals (like GaSe in Fig. 22) -- since the relevant k-vector components are those parallel to the surface, which remain unchanged. This had an impact beyond band mapping, stimulating attention on layer compounds – which later led to fundamental discoveries like graphene. Eventually, clever strategies extended band mapping to three-dimensional crystals.

Figure 23 illustrates an early example of photon-polarization-dependent photoemission. The differences between photoemission spectra taken with s-polarization and p-polarization, reflect the parity of the electronic states [52]. The theoretical analysis of Mike Schluter exploited them to identify the chemisorption geometry of Cl atoms on the cleaved Si(111) surface. The experimental apparatus had been boldly designed by the synchrotron spectroscopy pioneer John E. (Jack) Rowe: the polarization was switched by rotating the entire ultrahigh vacuum experimental chamber, a rather breathtaking maneuver!

Incidentally, this brings to light another important property of synchrotron radiation: its polarization [1]. Its causes can be easily grasped. For example, a bending magnet produces horizontal accelerations, so its radiation is linearly polarized in the horizontal plane. Likewise, undulators and wigglers cause transverse electron oscillations and also produce linear polarization.

But non-linear polarization can also be obtained. Above and below the horizontal plane, the emission becomes indeed elliptically polarized. One can understand why by realizing that, from tilted point of view, a trajectory inside a bending magnet looks like a portion of an ellipse. Unfortunately, because of its angular collimation the synchrotron radiation intensity sharply decreases when leaving horizontal directions. But elliptically polarized radiation with high intensity can be obtained with specially designed undulators that force the electrons to travel along spiral trajectories.

The impact of synchrotron radiation photoemission was not only practical but also deeply conceptual. For scientists of this writer's generation, photoemission experiments transformed bookish quantum notions into very tangible realities. The theoretical "Fermi energy" became a sharp edge in the photoemission spectra of metals; "core levels" corresponded to very visible

peaks; and the "band structures" were visualized by experimental plots. This author remembers the enthusiasm of Franco Bassani, a father of solid-state theory, when he saw the first experimental versions of his band structures!

Synchrotron photoemission progressively branched into new techniques and domains -- far too numerous to be listed here. As an example, we note photoelectron diffraction, pioneered by Alex Bradshaw, Phil Woodruff and Iggy McGovern [53] (all three authors of outstanding contributions to science, and Iggy also to poetry). Among the new domains, we note the very popular research on semiconductor interfaces, e.g., by the teams of Jack Rowe, Paolo Perfetti, Len Brillson [54], Bill Spicer [55], John Weaver [56], Alfonso Franciosi and others.

The next milestone in synchrotron photoemission was ultrahigh energy resolution, primarily – as mentioned - to study superconductivity. Figure 24 shows an early example by Yeukuang Hwu *et al.* [36], revealing the opening of the superconductivity gap in BSCO. The high-brightness of undulator sources also allowed high spatial resolution, as discussed in the later sub-section on spectromicroscopy.

Although photoemission played the leading role, other spectroscopy techniques did have an important impact on the history of synchrotron radiation. We would like to mention three examples: stimulated desorption, pioneered by Mort Traum and Norman Tolk [57], x-ray fluorescence spectroscopy and spectromicroscopy [58], and molecular spectroscopy.

This last application revolutionized molecular research, producing many fundamental advances. It was a key factor in the early establishment of synchrotron radiation research, and one of its fundamental components in the subsequent decades [58]. Among its pioneers at SRC, we note Jim Taylor, Tom Carlson, Manfred Krause and Maria Novella Piancastelli. The field also flourished at other facilities, most notably in France.

IV.2. Structural Techniques

Synchrotron spectroscopies mostly exploited the ultraviolet and "soft-x-ray" parts of the emission spectrum – roughly speaking, down to wavelengths of the order of 100 Å. In parallel, high-energy storage rings emitting hard-x-rays started another revolution: synchrotron

techniques for structural analysis at the atomic level. The revolution was primarily based on four classes of techniques: crystallography, powder diffraction, small-angle x-ray scattering (SAXS) and EXAFS (extended x-ray absorption fine structure) [1].

Crystallography had started, of course, much before synchrotron radiation, with Max von Laue's x-ray diffraction experiments in 1912, followed by those of the Bragg family (William Lawrence and William Henry) [59]. The conceptual background of x-ray diffraction is rather simple, but its practical implementation is affected by severe problems. In essence [1], the x-ray waves that are scattered in different directions by a given electron density distribution - *e.g.*, of a molecule - reflect its Fourier transform. After measuring the waves one could thus, in principle, perform a reverse Fourier transform and retrieve the distribution.

Let us consider x-ray scattering by a periodic crystal. The corresponding electron density distribution is determined by two concomitant factors: the distribution inside the crystal unit cell and the periodic crystal structure. Because of the properties of Fourier transforms, the crystal structure concentrates the diffracted x-rays into spots forming a regular pattern. From the pattern one can derive the crystal structure, and the spot intensities yield information on the charge distribution within the unit cell.

At present, these properties are mainly used to identify macromolecular structures. The macromolecules are arranged in crystals and constitute their unit cells [1,61-63]. Why using crystals instead of individual molecules? After all, crystallizing molecules is often a difficult and sometimes impossible task! The answer is that this strategy increases the signal-to-noise ratio by simultaneously probing many equivalent molecules, and makes more manageable the x-ray damage in individual molecules.

The practical implementation of macromolecular crystallography requires measuring pattern intensities for many different mutual orientations of the crystal and of the x-ray beam. This is needed to produce accurate and complete reverse Fourier transforms. Synchrotron sources facilitate the task, and are also very helpful in solving the ubiquitous "phase problem" [1,61-63].

Such a problem arises because the detected diffraction patterns do not really correspond to the x-ray waves but to their intensity, proportional to their square. Consider a simple plane

wave $A\exp[i(kx - \omega t + \phi)]$: the complex square is $|A|^2$ and does not depend on the phase factor. The measured intensity patterns, therefore, yield direct information on the wave amplitudes but not on the phases. However, the accurate retrieval of the electron density distribution requires both the amplitudes and the phases: this is the root of the "phase problem".

Before the advent of synchrotron radiation, the solutions were very complicated and time-consuming. For example, they could require [1,61-63] variants of the original crystal in which some specific atoms were replaced by heavy elements – increasing the difficulties related to crystal fabrication.

On the contrary, the leading solution based on synchrotron radiation – MAD (multi-wavelength anomalous diffraction) - does not necessitate atomic replacements. Its basic ingredient is "anomalous scattering", the rapid change of the scattering parameters with the wavelength that occurs near an x-ray absorption edge [1,61-64]. MAD requires taking diffraction patterns both at wavelengths close to the edge and far from it, thus the wavelength changes allowed by synchrotron sources are essential.

Synchrotron radiation plays an essential and widespread role in modern macromolecular crystallography – see for example Fig. 25 [64]. Synchrotrons are indeed used in a large portion of the macromolecular structure investigations, at least in the final step towards very accurate atomic structure determination.

The very broad applications of macromolecular crystallography triggered massive efforts for new techniques, dedicated beamlines and process automation. The brightness of synchrotron sources allows using very small crystals, reducing the difficulties of crystallization processes them and shortening the time required for each structure determination. The high source brightness also opens the door to the study of time-dependent structures.

Overall [61-63], macromolecular crystallography has become one of the pillars of modern synchrotron research and – as we shall see – a potential key customer for the new x-FEL's. The impact is very relevant not only for fundamental studies but also for applications – specifically, by the pharmaceutical industry.

X-Ray Powder Diffraction (XRPD) is another technique for which synchrotron sources made a revolutionary difference [65-67]. It works on systems consisting of microcrystals and on other materials with multiple microscopic orientations. As a consequence, their diffraction patterns are not formed by spots as for single crystals, but by circles.

Not requiring microscopically ordered systems, XRPD is more flexible than crystallography, although less accurate. It yields information on the chemical components of the specimen and their percentage, as well as on the microstructure [64-67]. It can be applied, in particular, to industrially important systems like solvates, polymorphs or amorphous specimens.

Synchrotron sources enhance the accuracy, power and flexibility of XRPD, improving its angular resolution, the signal levels and other performances, and shortening the acquisition time. With the best synchrotron sources, a complete XRPD characterization can now be performed with only a few micrograms of the analyzed substance – and within a time ranging from milliseconds to minutes [67].

Synchrotron XRPD has thus become a standard "working horse" for chemical and physical analysis with synchrotron radiation. The technique is also commercially available. Figure 26 shows an example: synchrotron XRPD results [67] produced by the Excelsus Structural Solutions Company founded by Fabia Gozzo.

When the specimen is disordered or partially ordered, crystallography can be also replaced by SAXS [1]. This class of techniques measures the scattered x-ray intensities only within a limited range of small angles. Because of the Fourier-transform properties, this reduces the capability to identify fine structural details. SAXS, therefore, is used to extract the general shape and relatively large features, on a typical scale of 10 Å.

The compensation for these limitations is that the technique does not require crystals and is, therefore, simpler to implement than crystallography. Using the so-called Guinier approximation [1], it can easily deliver general parameters like the "radius of gyration" -- a valuable initial information in the structural analysis of macromolecules.

In this case too, the high brightness of synchrotron sources and their capability to deliver monochromatic x-rays constitute great advantages. The angular collimation of the emission is

also an advantage. This is why SAXS beamlines have become a standard feature in modern synchrotron facilities.

The fourth main class of structural techniques using synchrotron radiation is based on EXAFS -- a weak modulation of the x-ray absorption coefficient that occurs over an extended range of photon energies above each absorption edge. These techniques played a key role in the transition from the first to the second generation of synchrotron sources [68-70].

The EXAFS history had actually started much before synchrotron radiation. In the early 1930's, Ralph Kronig [69] developed the theoretical background: the EXAFS modulation was indeed known as "Kronig structure" until the 1970's. But the practical applications were initially very difficult. The modulation is in fact very weak and its detection in the pre-synchrotron era required exceedingly long data taking times.

With the high intensity of synchrotron sources, fast experiments became practical [68] – solving in particular the problems of the x-ray intensity variations with time. The first tests of synchrotron EXAFS were performed in 1974 at SSRL (then known as SSRP, Stanford Synchrotron Radiation Project) by Peter Eisenberger, Dale Sayers, Edward Stern, Farrel Lytle, Brian Kincaid and Sally Hunter (Kincaid and Hunter were students of Artie Bienenstock) [70].

EXAFS techniques are important because they selectively measure local interatomic distances around the atoms a specific element. To understand how, consider a given photon energy absorption edge of a solid or a molecule. The edge is due to optical transitions between a core level and empty free-electron-like states with energies above the Fermi level or the bottom of the conduction band. Actually, the final states are not entirely free-electron-like, due to the effects of the atoms surrounding the "central atom" where the optical absorption takes place.

In a simplified picture (Fig. 27, left), one can model the final states as follows. After the photon absorption, the excited electron corresponds to an outgoing, spherical electron wave emanating from the central atom. But this wave is partially backscattered by the neighboring atoms: the excited-state electron wave is thus the combination of the outgoing and backscattered waves. Only backscattering from the closest neighboring atoms needs to be considered, since the excited electrons propagate over a very short distance before losing energy by inelastic scatterings.

Positive or negative interference of the outgoing and backscattered electron waves enhances or decreases the local wavefunction amplitude at the central atom site, and with it the optical-transition matrix element and the absorption coefficient. The interference depends on the interatomic distance and on the excited-electron wavelength – which in turn varies with the electron energy and therefore with the photon energy. As the photon energy increases, so does the excited-electron energy, decreasing the electron wavelength. Correspondingly, the interference goes from constructive to destructive, then again to constructive and so on, producing the EXAFS modulation [68].

The dependence on the local interatomic distances explains the importance of EXAFS techniques: from the modulation one can directly measure them. Neglecting for simplicity the backscattering-induced phase shift, positive interference occurs when $2d/\lambda_e = n$, where λ_e is the excited-electron wavelength and n is an integer number. Calling $k = 2\pi/\lambda_e$ the electron k-vector magnitude, this condition can be written as $4\pi kd = n$.

Thus, the EXAFS modulation is periodic with respect to k. A simple Fourier transform yields from it the interatomic distance d [68]. This can be selectively done for different chemical species by measuring and Fourier-transforming the EXAFS above the corresponding absorption edges.

EXAFS is, therefore, a powerful instrument largely complementary to crystallography. It offers the marked advantage of element selectivity. But it cannot reach a comparable accuracy in measuring atomic positions. EXAFS is particularly interesting when a minority of the chemical elements dominates the specimen properties. A widely used example is the case of hemoglobin and chlorophyll, which have similar structures but different atoms – iron or magnesium – at the center.

Due to their simplicity and flexibility, EXAFS techniques merit their status of key research instrument at all modern synchrotron facilities. They found over time a broad variety of applications: Fig. 27 (right) shows one of the earliest examples of synchrotron EXAFS [71].

EXAFS techniques are now very sophisticated and diversified, as many variations of the basic approach were successfully implemented. For example, measures of the fine structure in the

spectral regions near absorption edges – the so-called XANES (x-ray absorption near-edge fine structures) - are used [72] to explore chemical features, although the data analysis is less straightforward than for standard EXAFS. And EXAFS analysis can be performed with high surface sensitivity or on chemical species with very small concentrations.

IV.3. X-ray Imaging

This was the very first use of x-rays, inaugurated by Roentgen a few hours after his discovery: the radiography of his wife's hand is one of the icons of science history. The technology transfer to medical radiology was one of the most rapid ever. And imaging remains today, by far, the main field of x-ray activity.

It might be surprising, therefore, that the initial development of synchrotron-based radiology was not as fast as those of photoemission, EXAFS or crystallography. A few pioneers did start synchrotron imaging tests quite early (*e.g.*, the mammography initiative led by Emilio Burattini [72] in Frascati in the 1990's). But the development became rapid only after a stream of spectacular tomography results in the late 1990's and early 2000's [73-80].

The cause of the slow start was mainly conceptual. The superior quality of synchrotron imaging emerges when absorption contrast (which is weak for x-rays) is replaced by "phase contrast", allowed by high coherence. But, before synchrotron radiation, coherence was very difficult to achieve at short wavelengths, so most x-ray users neglected it.

Phase contrast is evident in images like those of Figs. 28 and 29 [73,81]: with the right conditions, it produces sharp edges of the object features that boost their visibility. One essential requirement [74,75] is a source with high "spatial coherence", i.e., with small size and emitting within a small angular range. One can understand why with very simple arguments [74,75]. In first approximation, the sharp edges are caused by the x-ray refraction at the corresponding boundaries between specimen regions. To detect these effects, one needs x-ray beams with well-defined directions. If the source area is too big and/or if it emits in a broad angular range, this condition is not fulfilled.

The quantity that measures spatial coherence is the "coherent power" [82]. We shall discuss later its foundations, anticipating here that it is proportional to the square of the wavelength divided by the source size and by its (two-dimensional) angular spread. Thus, obtaining a high coherent power is much more difficult for short-wavelength x-rays than for visible light.

Note that the same geometrical parameters – source size and angular divergence – determine both the coherent power and the brightness [1]. So, as the brightness was increased by improving the source geometry, so was the spatial coherence. Synchrotron sources of the second generation already reached high levels of coherent power -- although most users were unaware of this fact and missed excellent research opportunities.

All this changed in the early 2000-s [73-80], when synchrotron radiology became a leading activity at third-generation sources [83,84]. Figures. 28 and 29 show two examples of phase-contrast results from that period.

Figures 30 and 31 demonstrate [85,86] that the well-known medical technique "computer-assisted tomography" (CAT-scan) can be now extended to synchrotron phase-contrast radiology, producing spectacular three-dimensional reconstructed images. Tomography is implemented by taking many projection radiographs in different directions, with constant angular spacing. Then, computer algorithms are used to reconstruct from them the desired three-dimensional views of the specimen. Tomography is normally based on absorption contrast, but results like those of Fig. 30 and 31 show that now it extends to phase contrast.

Many other innovating synchrotron radiology techniques were developed, for example by David Chapman, Bill Thomlinson and their coworkers [83] and by the teams of Franz Pfeiffer and Marco Stampanoni [84]. But even in its simplest versions [74,75], phase contrast radiology yields images rich easily interpreted information. The applications now span from physics and chemistry to biology, materials science and medicine. And they were recently extended to cultural heritage – see the results of Fig. 32 by Fauzia Albertin *et al.* [87,88] - exploring for example sealed ancient manuscript written with "iron gall" ink.

IV.4. Microscopy and Spectromicroscopy

An important product of the high brightness of the third-generation synchrotron sources was a new class of techniques with high spatial resolution. The brightness yielded indeed the required signal-to-noise ratio to work on small specimen areas. This triggered the transition from x-ray imaging to microscopy, and from spectroscopy to spectromicroscopy – the combination of spectroscopy and high spatial resolution.

This evolution, however, encountered formidable technical obstacles. Most high-spatial-resolution techniques require focusing x-rays, which is very difficult [1]. The transmission lenses for visible light do not work at short wavelengths: in a large portion of their spectral range, x-rays are not transmitted by solids but absorbed. When they are transmitted, the refraction index is close to unity, making refraction optics ineffective. Focusing optics is an alternate solution, but x-ray reflection is very weak except for extreme glancing-incidence angles. This makes x-ray mirrors expensive and difficult to manufacture and operate.

These problems called for novel focusing techniques. Substantial progress was achieved by borrowing solutions that had been originally developed for visible light. These included [1], in particular, Schwarzschild objectives (Fig. 33) and Fresnel zone plates (FZP) (Fig. 34).

In the case of FZP's, their applications to x-rays required advanced microfabrication techniques. In fact, the radii of the circular transmitting and blocking zones are proportional to the square root of the wavelength [1,90]. Therefore, compared to a typical centimeter-size FZP for visible light, an x-ray FZP is much smaller, in the 100-μm range.

Since the spatial resolution is determined by the width of the outermost zone [1,90], the manufacturing process must be able to fabricate very narrow structures. But at the same time the absorbing zones must be thick enough to produce sufficient x-ray absorption. Thus, the outermost zones have a large "aspect ratio" (the thickness divided by the width), which can make them mechanically unstable.

Special designs and advanced fabrication techniques were finally able to tackle these problems, producing excellent progress in the x-ray FZP performances [90]. Similar progress was achieved for Schwarzschild lenses and other devices, with worldwide efforts.

Thanks to such advances, synchrotron microradiology produced results like those of Fig. 35 [91]. Such images changed the boundaries of radiology, initially conceived to analyze human organs with limited spatial resolution. Instead, as shown in Fig. 35 [91,92], the microradiology of today explores bio-structures down to individual cells and their components [92].

Figures 36 and 37 show two other examples of the current applications of synchrotron microradiology. The first experiment [93] explored the electrodeposition of Zn on a metal substrate. The high signal level allowed taking x-ray movies of the fast process, revealing a surprising phenomenon. The metal overlayer covered not only the solid substrate but also the fast-disappearing gas bubbles developed during electrodeposition. This verified a mechanism hypothesized long before, but quite hard to believe [93].

In Fig. 37, FZP microradiology reveals the channel system details in a firefly lantern [94]. The high spatial resolution allowed detecting even the smallest tubular structures. This was essential to reliably assess the quantitative gas exchanges during the emission of light – whereas previous microscopies could not detect very small vessels, missing a large part of the phenomenon. In turn, the accurate quantitative evaluations led to a fundamental advance in understanding the firefly emission, a fascinating and almost incredibly efficient phenomenon of nature [94].

Spatially resolved synchrotron techniques go beyond mere morphological analysis. As mentioned, combinations of spectroscopy and microscopy produced several synchrotron spectromicroscopies, capable of detecting not only the micromorphology but also local chemical and physical properties.

Relevant examples include x-ray fluorescence spectromicroscopy and micro-EXAFS. Figure 38 shows simplified schemes of two complementary approaches to photoemission spectromicroscopy. In the top one, lateral resolution is achieved by focusing the x-ray beam into a small spot – for example by a FZP. Photoelectrons are then collected at specific energies. By scanning the sample position on the transverse *xy* plane, one obtains two-dimensional photoemission intensity images. Suppose that the photoelectron energy corresponds to the core-level emission of a given chemical element: the images reflect its two-dimensional distribution. Figure 39 shows a nice example of these “microchemical pictures” [95].

In the approach of the bottom of Fig. 38 - called PEEM (photoelectron emission microscopy) [96-98] - the x-ray beam is not focused (or only weakly focused). High spatial resolution is achieved instead by processing the emitted photoelectrons with a suitable electron optics system. PEEM techniques were invented by pioneers like Brian Tonner and Ernst Bauer [96,97], and a nice example of their results is shown in Fig. 40 [98].

We personally witnessed the contributions to photoemission spectromicroscopy at SRC-Wisconsin and Elettra. These included the x-ray focusing instruments MAXIMUM and superMAXIMUM developed under Franco Cerrina's leadership [89], and the excellent PEEM-class instrument MEPHISTO constructed by P.U.P.A. Gilbert's team [98].

One particularly important element in the progress of PEEM was the photoelectron energy resolution. The early PEEM techniques did not include this capability: the "spectroscopic" aspects were implemented by scanning the photon energy. Later, several variants of PEEM achieved electron energy resolution, fully exploiting its potential [97]. In parallel, the spatial resolution also made great progress, yielding spectacular results -- see the image of Fig. 41 [99].

With the implementation of spectromicroscopy, synchrotron sources fully accomplished their historical missions -- becoming powerful and multi-faceted x-ray "microscopes" combining spatial resolution, energy resolution, morphological analysis, chemical investigations, physical analysis and, in some cases spin detection and/or time resolution. This revolution is still underway: the next chapter, discussed later, is the advent of x-FEL's.

IV.5. Applied Technologies

Applied research played a key but poorly understood role throughout the history of synchrotron radiation. Leading industrial entities like Bell Labs, Bellcore, IBM, Exxon, Xerox, and Martin-Marietta were present since the first generation of dedicated facilities. Synchrotron research produced many new applied techniques of industrial interest, many commercial products and a number of spinoff companies. Quite interestingly, the fabrication for sale of synchrotron instrumentation in Novosibirsk pioneered the transition from

communism to free-market economy in the Soviet Union, long before Gorbachev's Perestroika.

The industrial applications of synchrotron sources are multi-faceted. We already mentioned the use of XRPD. Likewise, many other synchrotron techniques are used by industry for characterization of materials and bio-systems – for example, proteins. Furthermore, synchrotron x-rays are exploited for manufacturing and for medical diagnostics and surgery.

X-ray lithography is the main synchrotron-based manufacturing technique [100]. It constitutes the evolution towards smaller features of ultraviolet lithography, the basic fabrication process in microelectronics. Improved miniaturization can be achieved, in principle, by decreasing the wavelength to the x-ray range. This implies using new types of photon sources, and also changing the fabrication process. In particular, it requires specialized photoresists such as PMMA (polymethylmethacrylate) [100].

For many years, the Wisconsin Center for x-Ray Lithography (CXrL) [101], founded by Franco Cerrina and supported by the industrial consortium Sematech, was the world leader in x-ray lithography. The implementation was successful, including interesting variants like the combination of lithography with LIGA (the German acronym for "Lithography-Electroforming-Replication") [102].

X-ray lithography is quite effective for specialized applications [100]. Can it expand, however, beyond niche uses? The question is still open, since it did not (or not yet) find widespread industrial applications. This is due to the progress of extreme ultraviolet lithography, which keeps pushing into the future the "time window" for x-ray fabrication.

Synchrotron sources successfully supported medical applications like coronary angiography [103], mammography [104] and brain surgery [105]. But the practical use for real cases was so far limited: medical doctors and patients are psychologically reluctant to use centralized synchrotron facilities. We should honestly admit that a synchrotron environment can be quite intimidating for a patient. A similar problem affected infrared FEL's: the Vanderbilt University Keck facility was very successful in experimental brain tumor surgery [105], but its operation was terminated before widespread applications.

In summary, synchrotron facilities are very successful in supporting industrial research and producing commercial instrumentation, but their role in fabrication, medical diagnostics and surgery is still not established. This is, in the author's opinion, a gold mine waiting to be fully exploited.

V. The Human Side

The history of synchrotron radiation is also, if not primarily, a saga of men and women who struggled against formidable obstacles, inspired by intuitions well ahead of their time. And also a tale of friendship, rivalry, joyful or humorous times (see Fig. 42) -- and in some cases tragedy. This writer would like to convey here a feeling about these human aspects, based on his own anecdotes.

Concerning tragedy, premature losses of good friends and outstanding scientists remain in the memory of synchrotron researchers of this writer's generation. We will commemorate a few of them in the acknowledgements.

Human aspects and personal relations were particularly important in the early days of synchrotron radiation, when resources were very limited and users assisted each other with instinctive solidarity and friendship. The scarcity of the means impacted the everyday life of the small synchrotron community. At the Wisconsin SRC, for example, the shortage of operators limited the Tantalus schedule to five days per week and nine hours per day. Exceptionally, an extra hour was "bought" with a case of beer for the machine staff.

Paradoxically, these schedule limitations were not negative: they left time for analyzing the data and discussing with the colleagues. In other words, for performing real experiments rather than merely taking data, as it is too often the case today.

Courage was a required and invaluable asset of the early users. They bet their professional future on facilities outside their control, building instruments and techniques more complex than most laboratory-based experiments. Courage was all the more remarkable for assistant professors, who gambled their future on synchrotron radiation while still in tenure-track.

The bureaucracy for getting beamtime was almost non-existent. At SRC, a request consisted in an oral interview with Ed Rowe, who initially looked at the postulant like a wealthy father hearing a penniless young man asking to marry his daughter. But, in the end, Ed was very friendly, in particular towards struggling young scientists.

Early users had to overcome technical obstacles and environmental hazards, from extremely cold weather in Wisconsin to earthquakes in Stanford, Berkeley and in Japan. And also more mundane difficulties. For example, the Tantalus building was very primitive, with only one restroom in the experimental floor. This caused a problem when Helen Farrell of Bell Labs became the first woman user: John Weaver found a bright solution, a two-sided sign for “Men” and “Women”.

Life on a beamline was often miserable. Before storage rings, the dangerous radiation of synchrotrons required shielding walls, built by hand-piling lead bricks – a dreadful task comparable to the Egyptian pyramid construction by slaves. At the early storage rings, the user teams were undersized, and humans performed many tasks later delegated to computers. Sleepless working periods of two or three days were not uncommon. And “sleeping” during data taking shifts often relied on very primitive facilities – such as mattresses on the experimental floor, as in Puzo’s “Godfather”.

During the intervals between beamtimes, lodging was similarly austere: by comparison, the “user guesthouses” of today are true luxuries. The arrangements ranged from sleeping inside parked cars to sharing the same hotel room and the same bed with other team members, using an alternating schedule that reflected the individual timetables (of course, no room cleaning for days).

Eating during beamtimes was totally unhealthy and largely based on junk food. The SRC coffee, an essential staple for handling the lack of sleep, was unspeakably awful: an agreement with the workers’ union had frozen the price per cup to the unreasonable level of five cents. In desperation and longing for a decent “espresso”, the Italian contingent used the abominable coffee, instead of water, to brew more coffee.

Notwithstanding all these difficulties and many others, the veterans of that period remember it with a nostalgic feeling. After all, we were all young and full of enthusiasm, all friends and all

unaffected by bureaucratic complications. And we had the exciting feeling of being part of a wonderful adventure, personally witnessing the birth of a great new field. We watched not only our own personal achievements, but also the milestones reached by our friends – and quickly put their results to good use for our own research.

I will conclude this short memoir with two anecdotes, tributes to the friendship and courage that marked the youth of synchrotron research. Concerning friendship, SRC was chronically short of money and could not afford the advanced equipment of its competitors. Yet, it became a birthplace of photoemission spectromicroscopy, using an outstanding but expensive undulator.

How did it manage? Thanks the gift of one of the Stanford undulators, arranged by the SSRL leader Herman Winick. SRC and SSRL were widely believed to be "adversaries", but the insiders know better: generosity and friendship marked their relations, as those of other synchrotrons worldwide. And these characteristics were certainly not limited to Herman Winick: other SSRL colleagues like Piero Pianetta and Ingolf Lindau distinguished themselves for gentlemanship.

About courage: when the commissioning of the second SRC source Aladdin was hit by technical difficulties, the granting agency in Washington prematurely decided to shut it down. And rudely ordered the SRC director of that time, Dave Huber, to move all its beamlines back to Tantalus, which was an obsolete facility. Dave defiantly responded by moving instead all beamlines from Tantalus to Aladdin, betting on its final victory. This brave stance was crucial to the success of Aladdin -- and to its three decades of outstanding contributions to science and technology.

VI. A Very Bright Future

We now reach the present phase of our history, with revolutionary strategies to boost the brightness of storage ring (with the multiple-bend achromat lattices spearheaded by Mike Eriksoon and Dieter Einfeld [15]) and above all with the advent of x-FEL's and their first experiments. For the reasons previously illustrated, the FEL technology - invented by John Madey in 1971 [106] - remained confined for four decades to infrared wavelengths [7-10].

The theory of x-FEL's was proposed in the 1980's, notably by Claudio Pellegrini in the SASE version [11]. But it took an exceedingly long time to transform it into practical machines.

The first x-FEL, LCLS, was commissioned at SLAC in 2009 [12]. Other facilities followed: FLASH at DESY, FERMI at Elettra, SACLA at Spring-8. And advanced projects are now underway in several countries.

The performances of these facilities defy the imagination: their peak brightness (Fig. 18) surpasses the best storage rings by many orders of magnitude; the pulse duration is as short as a few femtoseconds; and each pulse packs up to several mJ of electromagnetic energy in a very small volume. Such pulses are thus unprecedented physical systems, which support novel experimental techniques and will perhaps unveil new physics.

The short pulse duration can be effectively exploited for time-dependent experiments down to femtoseconds. An interesting case is the one-shot analysis of molecular or nanoparticle atomic structures [107-110], an alternate strategy to crystallography. Suppose that a powerful x-FEL pulse is sent into a nanoparticle or a macromolecule: as illustrated in Fig. 43, it destroys the specimen. However, if the pulse is short enough it can produce a transient diffraction pattern, from which one can extrapolate the structure before destruction. This could eliminate the need for crystals, or at least for large crystals, simplifying the identification of macromolecular and nanoparticle structures.

The first tests were recently presented – see for example Refs. 107-110 – but this approach is still far from routine. Figures 44 and 45 show two recent cases [109,111]. The forthcoming years will tell us to what extent this strategy can complement and/or partly replace traditional crystallography.

The exceptional peak brightness and short duration of the x-FEL pulses open up many other novel research avenues – such as the dynamic study of ultrafast phenomena. Figure 46 shows an exciting recent example. The inset illustrates a Frank-Condon optical transition in molecular iodine, reaching excited electronic and vibrational states. Using the LCLS x-FEL at Stanford and very clever experimental solutions, the authors of [112] detected the subsequent molecular evolution on the scale of a few angstroms and over a time range of picoseconds.

The accumulated results on many molecules revealed the vibrational oscillations after the optical excitation (region b in Fig. 46). But they also detected a wealth of other phenomena, including dissociation (c) and rotational dephasing (e). The x-FEL's are thus, once again, transforming theoretical quantum notions into tangible experimental realities.

VI.1. Coherence

The x-FEL's reach unprecedented levels of spatial coherence and now, thanks to seeding, also excellent time ("longitudinal") coherence. We already introduced spatial coherence to discuss phase contrast. But, in the context of x-FEL's, both spatial and time coherence deserve a more detailed discussion.

What is coherence? A simple way to respond is with Heisenberg's uncertainty principle, which makes it impossible to experimentally prove both the particle nature and the wave nature of electromagnetic radiation, simultaneously and with infinite accuracy.

One can prove the wave nature by detecting phenomena like interference and diffraction. And "coherence" is the property that allows observing such phenomena. Spatial coherence and time coherence are complementary aspects of this property.

Starting from spatial coherence, consider the example of Fig. 47: a square-shaped electromagnetic radiation source illuminating an absorbing screen with two slits at a very close distance d from each other. Will the radiation produce a detectable interference pattern, as shown in Fig. 47? This requires its wave nature to prevail over the particle nature. Specifically, if the interference pattern is detected, then the Heisenberg principle forbids to accurately prove the passage of individual photons through only one slit.

This means that the uncertainty Δx in the radiation position along the transverse x-axis must be larger than d. Heisenberg's principle tells us that:

$$\Delta x \approx \frac{h}{\Delta p_x},$$

where h is the Planck constant. And, considering all the possible trajectories of radiation from the source, the maximum uncertainty for the transverse momentum is:

$$\Delta p_x \approx \frac{\Sigma_x}{L} p = \frac{\Sigma_x}{L} \frac{h}{\lambda},$$

where L is the source-screen distance, $2\Sigma_x$ the source size along x, (Σ_x/L) the order of magnitude of the maximum angle of the rays with respect to the forward z-direction, and $p = h/\lambda$ is the momentum magnitude. Thus, the condition for seeing the pattern becomes:

$$d < \Delta x \approx \frac{h}{\Delta p_x} \approx \frac{h}{\left(\frac{\Sigma_x}{L}\right)\left(\frac{h}{\lambda}\right)},$$

or:

$$d < \frac{\lambda L}{\Sigma_x}.$$

This means that only radiation reaching the screen within a lateral x-range $\approx \lambda L/\Sigma_x$ can produce wave-like phenomena like interference. This is the radiation with spatial coherence.

By repeating the analysis for the y-direction (after rotating by $\pi/2$ the two slits) and calling $2\Sigma_y$ the source size along y,, we see that the radiation is spatially coherent over an area:

$$S_c = \frac{\lambda L}{\Sigma_x} \frac{\lambda L}{\Sigma_y} = \frac{\lambda^2 L^2}{\Sigma_x \Sigma_y},$$

the so-called "coherence area".

If the angular spreads of the source emission in the x and y-directions are larger than (Σ_x/L) and (Σ_y/L), not all the radiation reaches S_c. Calling Ω_x and Ω_y the emission angular spreads along x and y, the fraction that does is:

$$\approx \frac{S_c}{(L\Omega_x)(L\Omega_y)} = \frac{\lambda^2}{\Sigma_x \Sigma_y \Omega_x \Omega_y}.$$

This defines the (spatial) "coherent power" of the source – the parameter that we already used to discuss phase contrast.

By decreasing the source size and its angular divergence, synchrotrons and then x-FEL's progressively reached higher levels of coherent power. But there exist an absolute limit for this increase. Imagine a small source obtained by placing a opaque screen with a circular pinhole of diameter 2Σ along the path of a plane wave. If 2Σ is very small, diffraction effects cause an angular spread Ω of the order of λ/Σ. Thus, for each transverse direction the product $\Sigma_x\Omega_x$ or $\Sigma_x\Omega_y$ cannot be smaller than $\approx\lambda$, and the ratio determining the spatial coherent power, $\lambda^2/(\Sigma_x\Sigma_y\Omega_x\Omega_y)$, cannot be larger than ≈ 1.

This "diffraction limit" for spatial coherence is not a technical feature, but a fundamental property of nature. When it is reached, the source possesses full spatial coherence. Some third-generation synchrotrons already achieved full spatial coherence over part of their emission spectrum. And the x-FELs of today do even better.

We shall now consider time coherence, using again Fig. 47. To observe the interference pattern, the radiation reaching the slits must behave as a wave rather than as a collection of individual photon pulses. If the pulse longitudinal width Δz is zero, no pattern is observed. For sufficiently large Δz–values, the pattern becomes visible.

The condition for shifting from "photons" to "wave" is, obviously, that Δz is large enough to include wave-like oscillations: $\Delta z > \lambda$. For very close slits:

$$p_z \approx p = \frac{h}{\lambda},$$

and:

$$\Delta p_z \approx \left|\frac{dp_z}{d\lambda}\right| \Delta\lambda \approx \left|\frac{d(h/\lambda)}{d\lambda}\right| \Delta\lambda \approx h\frac{\Delta\lambda}{\lambda^2},$$

so, using Heinseberg's principle in the longitudinal direction, $\Delta z \Delta p_z \approx h$:

$$\Delta z \approx \frac{h}{\Delta p_z} \approx \frac{\lambda^2}{\Delta\lambda} ,$$

and $\Delta z > \lambda$ implies $\lambda/\Delta\lambda > 1$. This is the minimal condition for time coherence.

The above derivation implies that $\Delta z \approx \lambda^2/\Delta\lambda$ is the Heisenberg uncertainty in the longitudinal position of each photon. So, when the distance between two photon pulses is $<\lambda^2/\Delta\lambda$, they cannot be distinguished from each other as individual particles – and the radiation can produce wave-like phenomena such as interference. The distance

$$L_c = \frac{\lambda^2}{\Delta\lambda}$$

is thus the "coherence length", within which the photons are indistinguishable and the radiation possesses time coherence.

Combined together, S_c and L_c define the "coherence volume":

$$V_c = S_c L_c = \frac{\lambda^2 L^2}{\Sigma_x \Sigma_y} \frac{\lambda^2}{\Delta\lambda} = \frac{\lambda^4 L^2}{\Sigma_x \Sigma_y \Delta\lambda} ;$$

within V_c, Heisenberg's principle does not allow photons to be detected as independent particles, so they act coherently producing wave-like effects.

The ultimate objective in constructing coherent x-rays sources is to put a lot of radiation energy inside V_c. This facilitates all experiments based on coherence, and opens the door to new applications. For example, speckle-based techniques [113] can be easily implemented, notably when the specimen is smaller than the coherence volume.

VI.2. Seeding

This is a very important recent development of x-FEL's [114-117] that solves a serious problem affecting the SASE mechanism [11]. In SASE, the amplification concerns photon pulses spontaneously emitted by the electrons when they enter the insertion device. This initial emission is stochastic, with strong fluctuations between the individual x-FEL pulse shapes. The time coherence of SASE x-FEL's is thus limited, in contrast with their excellent lateral coherence. The pulse-to-pulse fluctuations notably handicap time-dependent experiments.

With seeding, the x-FEL process amplifies, instead of the random spontaneous emission, well-controlled pulses from an external laser [116]. The realization of seeding is not trivial, since conventional lasers cannot yield hard-x-ray wavelengths. Figure 48 shows the solution adopted in the FERMI FEL-1 source, which exploits HGHG ("high-gain harmonic generation") [116].

In the simplified scheme of this figure, an external laser pulse of medium wavelength is injected in the x-FEL synchronously with a previously accelerated and compressed electron bunch. Within the "modulator" section (the combination of an energy-modulating undulator and of a chromatic dispersion section [116]), the electron-photon interaction spatially modulates the electron bunch. The apparatus is designed to produce a modulation not only with the fundamental wavelength periodicity, but also with strong higher harmonics.

Traveling along the specially designed long "radiator" insertion device, the electron bunch produces progressively amplified radiation with wavelength equal to one of the higher harmonics. This effectively converts the medium wavelength of the external laser into short-wavelength pulses. Their time characteristics are controlled by the seeding pulses and immune from the SASE problems. Practical HGHG x-FEL's use of course more complicated schemes than Fig. 48, with multiple stages that produce very short wavelengths.

An alternate version of seeding technique uses, instead an external laser, the radiation emitted by a first SASE x-FEL section. The SASE pulses are filtered by a monochromator, narrowing their wavelength bandwidth, before being injected into the main x-FEL section for optical amplification.

A hypothetical scheme until recently, seeding is now an exciting reality. Figure 49 shows, for example, the output of the seeded FERMI x-FEL HGHG source. Note the excellent pulse-to-pulse stability.

In conclusion, seeding is unlocking the full potential of x-FEL's, opening a new era in synchrotron radiation history. The future looks, once again, very bright!

VII. A Revolution in Research

Synchrotron radiation sources, together with neutron facilities, caused deep cultural changes in condensed matter research. Previously, large accelerators had triggered a similar revolution in particle physics. Small-scale projects had been replaced by giant experiments at centralized facilities, involving very large teams. The consequences extended well beyond elementary particle research – and science in general.

Indeed, the need to effectively communicate within huge, geographically delocalized teams stimulated the creation of the World Wide Web and Internet [118]. Branching outside elementary-particle physics, Internet revolutionized the world economy and our society, with far-reaching effects on our everyday life – from politics to commerce and from social relations to – alas - terrorism and crime.

In elementary particle research, the new culture required major strategic adjustments. And the effective training of new generations, not only in physics and technology but also in management, finances and public relations. Our elementary particles colleagues did an excellent job in meeting these challenges. This explains why accelerators were first developed for elementary particles rather than for synchrotron radiation -- as futilely imagined in our fictional tale.

The similar, recent revolution in condensed matter research was not as complete as for elementary particles, nor with comparable implications. Still, it was very important and far-reaching.

What are its components? First, a radical change in the research planning and implementation. Performing experiments at a big centralized facility, faraway from the home institution, is a challenging task. It typically requires coordinating a large team with an effective and stringent distribution of objectives and duties – and with very effective internal communications. The scarcity of synchrotron beamtime forces the users to be exceedingly professional in their strategies. Good planning and engineering must support the experiments, since failures due to negligence or insufficient preparation are not forgiven and can lead to disastrous career consequences.

These realities also impact education. Doctoral candidates performing their research at synchrotron facilities are trained in an environment similar to the "real" world. Thus, they are well prepared for the competitive work environment of today.

Is this cultural revolution positive or negative? The fans of "small science" look back with nostalgia at the "good old days", regretting the shift to "big science". But such nostalgic feelings are, in this writer's opinion, unrealistic. The transition to large facilities is not "good" or "bad", but a reality caused by the natural evolution of condensed matter research. And fighting against historical realities is not a good choice for a scientist.

As all revolutions, synchrotron radiation has of course negative aspects – like the difficulty in running real experiments during the limited beamtime. But even the staunchest supporters of "small science" must recognize its many positive aspects.

Synchrotron facilities are notably open to all qualified users based on merit, with no financial charges and sometimes with support for travel and lodging expenses. Note, in particular, the series of effective programs supported by the European Commission to financially assist transnational users [119]. Good scientists in less-favored countries are thus able to realize their full potential without emigrating. The impact is particularly positive for young researchers, women scientists and minorities: the merit selection for access to synchrotron facilities is fully immune from discriminations.

The above cultural revolution is now extending to the life sciences. Other factors contribute to this development, like "big data" techniques and massive computer modeling. But synchrotron-based techniques do play a key role. And we witness once again resistance

against the new trends, which has caused serious damage to excellent “big-science” projects [120] in biology. But time will take care of this problem.

Indeed, the younger generations are fortunately open to the culture created by elementary particle research, synchrotrons and FEL’s. A culture of effectiveness, accountability, good planning and training, strict merit selection, equal opportunities and objective fairness.

This will be, in this author’s opinion, the longest-lasting legacy of many very successful decades of synchrotron radiation research.

Acknowledgments

The author is deeply grateful to two groups of colleagues who played a key role in his five decades of synchrotron radiation activities. First, the many outstanding researchers with whom he collaborated, in particular the members of his experimental teams. Second, the technical experts who developed and operated the facilities he used: accelerator scientists and beamline specialists.

Mentioning all of them would be well deserved but impossible. We will just name (with my apologies to the others) the operation manager of Tantalus and Aladdin, Roger Otte, symbol of many others that made – and make - synchrotron experiments possible for external users throughout the world. And Charlie Pruett, head of the SRC optics group. And five outstanding leaders of accelerator science: Albin Wrulich, Mario Puglisi, Lenny Rivkin, Claudio Pellegrini and, of course, Ed Rowe. Without them and their many colleagues, the revolution of synchrotron radiation would have never happened.

Unfortunately, some of these colleagues are no longer with us: Otte, Spruett, Puglisi, Rowe. We remember them with reverence and admiration, together with others who left us prematurely: Ernst Ekhard Koch (pioneer and leader of DESY-HASYLAB and BESSY), Franco Cerrina, Mort Traum (co-inventor of angle-resolved photoemission). And Werner Meyer-Ilse, an outstanding x-ray optics expert from the Lawrence Berkeley Laboratory. And Adolfo Savoia, Carlo Coluzza and Hartmut Hochst, friends and co-workers of this writer for many years. In their memory, and also to honor all the others whom we could not mention here, we propose Ed Rowe's preferred quotation from Shakespeare:

"*… yet all shall be forgot,*
But he'll remember, with advantages,
What feats he did that day."

References

[1] Margaritondo G., *Introduction to Synchrotron Radiation* (Oxford, New York) 1988; Margaritondo G., *Elements of Synchrotron Light for Biology, Chemistry, and Medical Research* (Oxford, New York) 2002.

[2] Winick H., *Synchrotron Radiation Sources: a Primer* (World Scientific, Singapore) 1995.

[3] Willmott P., *An Introduction to Synchrotron Radiation Techniques and Applications* (Wiley, New York) 2011; Mobilio, S., Boscherini F. and Meneghini C., *Synchrotron Radiation Basics, Methods and Applications* (Springer, Berlin) 2015.

[4] Bordovitsyn V. A., *Synchrotron Radiation Theory and its Development*, Series on *Synchrotron Radiation Techniques and Applications*, Vol. **5** (Springer, Berlin) 1999.

[5] Wiedemann H., *Synchrotron Radiation* (Springer, Berlin) 2003.

[6] http://www.lightsources.org/regions

[7] Margaritondo G. and Rebernik Ribic P., *J. Synchrotron Radiation* **18** (2011) 101; Rebernik Ribic P. and Margaritondo G., *Phys. Stat. Solidi* **249** (2012) 1210; *J. Phys. D* **45** (2012) 213001.

[8] Saldin E. L., Schneidmiller E. A. and Yurkov M. V., *The Physics of Free Electron Lasers* (Springer, Berlin) 2000.

[9] Gawelda W., Szlachetko J., Milne C. J., *X-ray spectroscopy at X-ray Free Electron Lasers*, in *XAS and XES; Theory and Applications*, Edited by van Bokhoven J. A. and Lamberti C., (Wiley, New York) 2015.

[10] Brau C. A., *Free Electron Lasers* (Academic Press. New York) 1990.

[11] Pellegrini C., *Rev. Accl. Sci. Tech.* **3** (2010) 185; Bonifacio R., De Salvo L., Pierini P., Piovella N. and Pellegrini C., *Phys. Rev. Lett.* **73** (1994) 70.

[12] Emma, P*. et al., Nat. Photon.* **4** (2010) 641.

[13] Attwood D., Halbach K. and Kim K. J., *Science* **14** (1985) 1265.

[14] Bernardini C., Corazza G. F., Di Giugno G., Ghigo G., Haissinski J., Marin P., Querzoli R. and Touschek B., *Phys. Rev. Lett.* **10** (1963) 407.

[15] Robinson A. L., in *X-Ray Data Booklet*, Edited by Thompson A. C. (Lawrence Berkeley National Laboratory, Berkeley) 2009, pp. 21-28; Erikkson M. and Einfeld D., CERN Courier, August 12, 2016 issue.

[16] Pollock H. C., *Am. J. Phys.* **51** (1982) 278; Elder F. R. et al., *Phys. Rev.* **71(**1947) 829.

[17] Mottana A. and Marcelli A., *J. Synchrotron Radiation* **20** (2013) 811.

[18] Margaritondo G., *Physics Today* **61** (2008) 37.

[19] Rowe E. M., http://www.src.wisc.edu/about/erowe.htm.

[20] Rowe E. M. and Mills F. E., *Particle Accelerators* **4** (1973) 211.

[21] Lynch D. W., *J. Synchrotron Radiation* **4** (1997) 334.

[22] Lynch D. W., Plummer W., Himpsel Fr., Chiang T. C., Margaritondo G. and Lapeyre G. J., *Synchrotron Radiation News* **28** (2015) 20.

[23] Cole F. T., http://accelconf.web.cern.ch/AccelConf/c01/cyc2001/extra/Cole.pdf.

[24] Pomeranchuk I. Ya., *JETP* **9** (1939) 915; Ivanenko D. D. and Pomeranchuk I. Ya., *Phys. Rev.* **65** (1944) 343; Artsimivich L. A. and Pomeranchuk I. Ya., *JETP* **16** (1946) 379.

[25] Schwinger J., *Phys. Rev.* **70** (1949) 1912.

[26] Veksler V. I., Dokladi **43** (1944) 329; McMillan E. M., *Phys. Rev.* **68** (1945) 143.

[27] Tomboulian D. H. and Hartman P. L., *Phys. Rev.* **102** (1956) 1423.

[28] Madden R. P., in *X-ray Spectroscopy*, edited by Azaroff L. V. (McGraw-Hill, New York) 1974, pp. 338-378.

[29] Cauchois Y., Bonnelle C., and Missoni G., *Comptes Rendus. Acad. Sci. Paris* **257** (1963) 409.

[30] Balzarotti A., Bianconi A., Burattini E. and Strinati G., *Solid State Commu*n. **15** (1974) 1431.

[31] Balzarotti A., Piacentini M. and Grandolfo M., *Lett. Nuovo Cimento* **3** (1970) 15.

[32] Bernardini C., *Phys. Perspect.* **6** (2004) 156.

[33] Amaldi E., *The Bruno Tousheck Legacy* (CERN, Geneva) 1981.

[34] Augustin J.-E. *et al.*, *Phys. Rev. Lett.* **33** (1974) 1406.

[35] Sanchez del Rio M., Canestrari N. and Cerrina F., *J. Synchrotron Radiation* **18** (2011) 708.

[36] Hwu Y. et al., *Phys. Rev. Lett.* **67** (1991) 2573.

[37] Margaritondo G., in *The Gap Symmetry and Fluctuations in High-T_C Superconductors*, edited by Bok J., Deutscher G., Pavuna D. and Wolf S. A. (Plenum, New York and London) 1998, p. 195.

[38] Kelley R. J., Ma J., Margaritondo G. and Onellion M., *Phys. Rev. Lett.* **71** (1993) 4051.

[39] Margaritondo G. and Weaver J. H., in *Methods of Experimental Physics - Vol. 22 (Surfaces)*, edited by Park R. L. and Lagally M. J. (Academic Press, New York) 1985, Chapter 3.

[40] Margaritondo G., in *Physics and Chemistry of Materials with Low Dimensional Structure - Electronic States and Electronic Transitions in Layer Materials*, edited by Grasso V. (Reidel, Dordrecht) 1986, Vol. 20, Chapter 6; Margaritondo G. in *Highlights on Spectroscopies*

of Semiconductors and Insulators, edited by Balzarotti A., Guizzetti G. and Stella A. (World Scientific, Singapore) 1989, p. 387.

[41] Coluzza C., Sanjinés R. and Margaritondo G., *Photoemission: from the Past to the Future* (EPFL, Lausanne) 1992.

[42] Einstein A., *Ann. Phys.* **17** (1905) 132.

[43] Lapeyre G. J., Smith R., Knapp J. and Anderson J., *Journal de Physique Colloques* **39** C4 (1978) 134.

[44] Lapeyre G. J. *et al.*, *Solid State Commun.* **15** (1974)1 601.

[45] Lapeyre G. J., Anderson J., Gobby P. L. and Knapp J., *Phys. Rev. Lett.* **33** (1974) 1290.

[46] Margaritondo G., Rowe J. E. and Christman S. B., *Phys. Rev.* **B15** (1977) 3844.

[47] Haensel R. *et al., Phys. Rev. Lett.* **23** (1969) 530.

[48] Gudat W. and Kunz, C. *Phys. Rev. Lett.* **29** (1972) 169.

[49] Margaritondo G., Franciosi A., Stoffel N. G. and Edelman H. S., *Solid State Commun.* **36** (1980) 297.

[50] Smith N. V., Traum M. M., Knapp J. A., Anderson J. and Lapeyre G. J., *Phys. Rev.* **B13** (1976) 4462.

[51] Larsen P. K., Margaritondo G., Rowe J. E., Schluter M. and Smith N. V., *Physics Letters* **58A** (1976) 423.

[52] Schluter M., Rowe J. E., Margaritondo G., Ho K. M. and Cohen M. L., *Phys. Rev. Lett.* **37** (1976) 1632.

[53] Franco N. *et al., Applied Surface Science* **123/124** (1998) 219; Giessel T. *et al., Surface Science* **406** (1998) 90.

[54] Brillson L. J., *Surf. Sci. Rep.* **2** (1982) 123.

[55] Spicer W. E., Lindau I., Skeath P., Su C. Y. and Chye P., *Phys. Rev. Lett.* **44**, (1980) 420.

[56] Xu F., Vos M., Weaver J. H. and Cheng H., *Phys. Rev.* **B 38** (1988) 13418.

[57] Tolk N. H. *et al., Phys. Rev. Lett.* **49** (1982) 812.

[58] Beckhoff B., Kanngiesser B., Langhoff N., Wedell R. and Wolff H., *Handbook of Practical X-ray Fluorescence Analysis* (Springer, Berlin) 2006.

[59] Carlson T. A. *et al., J. Chem. Phys.* **81** (1984) 3828, and the references therein.

[60] Friedrich W., Knipping P. and von Laue M., *Sitzungsberichte der Mathematisch-Physikalischen Classe der Königlich-Bayerischen Akademie der Wissenschaften zu München* (1912) 303; Bragg W. L., *Proc. Cambridge Philosophical Society* **17** (1913) 43.

[61] Hendrickson W. A., *Rev. Biophys.* **47** (2014) 49.

[62] Wlodawer A., Minor W., Dauter Z. and Jaskols M., *FESB Journal* **280** (2013) 5705.

[63] Helliwell J. R. and Mitchell E. P., *IUCrJ* **2** (2015) 283.

[64] Ban, N., Nissen, P., Hansen, J., Moore, P. B. and Steitz, T. A., *Science* **289** (2000) 905.

[65] Gozzo F., in *Uniting Electron Crystallography and Powder Diffraction*, edited by Kolb U., Shankland K., Meshi L., Avilov A. and David W. I. F. (Springer, Dordrecht) 2012, p. 65.

[66] Lavina B., Dera P. and Downs R. T., *Reviews in Mineralogy and Geochemistry* **78** (2014) 1.

[67] Fili S. *et al.*, IUCrJ **2** (2015) 535.

[68] Stern E. A., *J. Synchrotron Radiation* **8** (2001) 49.

[69] Kronig R. de L., *Z. Phys.* **70** (1931) 317; Kronig R. de L., *Z. Phys.* **75** (1932) 191; Kronig R. de L., *Z. Phys.* **75** (1932) 468.

[70] Eisenberger P., Kincaid B., Hunter S., Sayers D., Stern E. A. and Lytle F., in *Proceedings of the IV International Conference on Vacuum Ultraviolet Radiation Physics*, edited by Koch E. E., Haensel R. and Kunz C. (Pergamon, Oxford) 1974, p. 806.

[71] Eisenberger P. et al., *J. Nature* **274** (1978) 30.

[72] Burattini E. *et al.*, *Radiology* **195** (1995) 239.

[73] Meuli R., Hwu Y., Je J. H. and Margaritondo G., *Europoean Radiology* **14** (2004) 1550.

[74] Margaritondo G. and Tromba G., *J. Appl. Phys.* **85** (1999) 3406.

[75] Hwu Y. et al., *J. Appl. Phys.* **86** (1999) 4613.

[76] Arfelli F. *et al.*, *Phys. Med. Bio.* **42** (1998) 2845.

[77] Chapman D. *et al.*, *Phys. Med. Biol.* **42** (1997) 2015

[78] Pogany A., Gao D. and Wilkins S. W., *Rev. Sci. Instrum.* **68** (1997) 2774.

[79] Hwu Y. and Margaritondo G., *J. Phys D* **46** (2013) 490301.

[80] Margaritondo G., Hwu Y. and Je J. H., *Sensors* **8** (2008) 8378.

[81] Hwu Y. et al., *Biophysical J.* **87** (2004) 4180; Hwu Y. *et al.*, unpublished data.

[82] Attwood D., *Soft X-Rays and Extreme Ultraviolet Radiation: Principles and Applications* (Cambridge University Press, Cambridge) 2007.

[83] Dilmanian F. A. *et al.*, *Phys. Med. Biol.* **45** (2000) 933.

[84] McDonald S. A. *et al.*, *J. Synchrotron Radiation* **16** (2009) 562.

[85] Hwu Y. *et al.*, unpublished data.

[86] Chien C. C. *et al.*, *Biotechnology Advances* **31** (2013) 396; Margaritondo G. and Hwu Y., *Nuovo Saggiatore* **29** (2013) 45.

[87] Albertin F. *et al.*, *X-ray Spectrometry* **44** (2015) 93.

[88] Albertin F. *et al.*, *J. Synchrotron Radiation* ***22*** (2015) 445.

[89] Cerrina F. *et al., Rev. Sci. Instrum.* **60** (1989) 2249; Cerrina F. et al., *J. Vac. Sci. Technol.* **A8** (1990) 2563.

[90] Chen Y. T. *et al., Nanotechnology* **19** (2008) 395302.

[91] Wu H. R. *et al., J. Phys. D* **45** (2012) 242001.

[92] Meyer-Ilse W. *et al., J. Microscopy* **201** (2000) 395.

[93] Tsai W. L. *et al.,* Nature **417** (2002) 139.

[94] Tsai Y. L. *et al.,* Phys. Rev. Lett. **113** (2014) 258103.

[95] Bozzini B. et al., *J. Phys. Chem.*. **C 116** (2012) 7243.

[96] Tonner B. P. and Harp G. R., *Rev. Scientific Instrum.* **59** (1988) 853; Tonner B. P. and Harp G. R., *J. Vacuum Sci. Technol.* **A7** (1992) 1; Tonner B. P., Harp G. R., Koranda S. F. and Zhang J., *Rev. Scientific Instrum.* **63** (1992) 564.

[97] Bauer E., *Ultramicroscopy* **119** (2012) 18.

[98] Johnson C. J. *et al., Viruses* **5** (2013) 654; De Stasio G. *et al., Rev. Sci. Instrum.* **69** (1998) 2062; De Stasio G. *et al., Rev. Sci. Instrum.* **69** (1998) 3106.

[99] Robinson J. T. *et al., Nano Letters* **7** (2007) 2655.

[100] Cerrina F., in Handbook of *Microlithography, Micromachining and Microfabrication, Vol. 1: Microlithography*, edited by Rai-Choudhury P. (Society of Photo-Optical Instrumentation Engineers (SPIE), Bellingham) 1997, p. 251.

[101] Cerrina F., *Synchrotron Radiation News* **2** (1990) 15.

[102] Saile V., *LIGA and its Applications* (Wiley, Hoboken) 2009.

[103] Rubenstein E., *Ann. Rev. Biophys. Biophys. Chem.* **16** (1987) 161.

[104] Castelli E. *et al., Radiology* **259** (2011) 684.

[105] Edwards G. *et al., Nature* **371** (1994) 416.

[106] Madey J. M. J., *J. Applied Phys.* **42** (1971) 1906.

[107] Chapman N. H. *et al., Nature Physics* **2** (2006) 839.

[108] Chapman N. H. *et al., Nature* **448** (2007) 676.

[109] Chapman N. H. *et al., Nature* **470** (2011) 73, and the references therein.

[110] Ekeberg T. *et al., Scientific Data* **3** (2016) 160060, and the references therein.

[111] Ekeberg T. *et al., Phys. Rev. Lett.* **114** (2015) 098102.

[112] Glownia J. M. *et al., Phys. Rev. Lett.* **117** (2016) 153003.

[113] Langeler B., *Naturwissenschaften* **88** (2001) 249.

[114] Yu L. H., *Phys. Rev.* **A 44** (1991) 5178.

[115] Amann J. *et al., Nature Photonics* **6** (2012) 693, and the references therein.

[116] Allaria E. *et al., Nature Photonics* **6** (2012) 699, and the references therein.

[117] Bocchetta C. J. *et al., FERMI@Elettra FEL Conceptual Design Report* (Sincrotrone Trieste) 2007.

[118] Berners-Lee T., *Information Management : a Proposal* (CERN, Geneva) 1989.

[119] Berrier E. *et al., J. Synchrotron Radiation* **21** (2014) 638.

[120] https://www.humanbrainproject.eu/

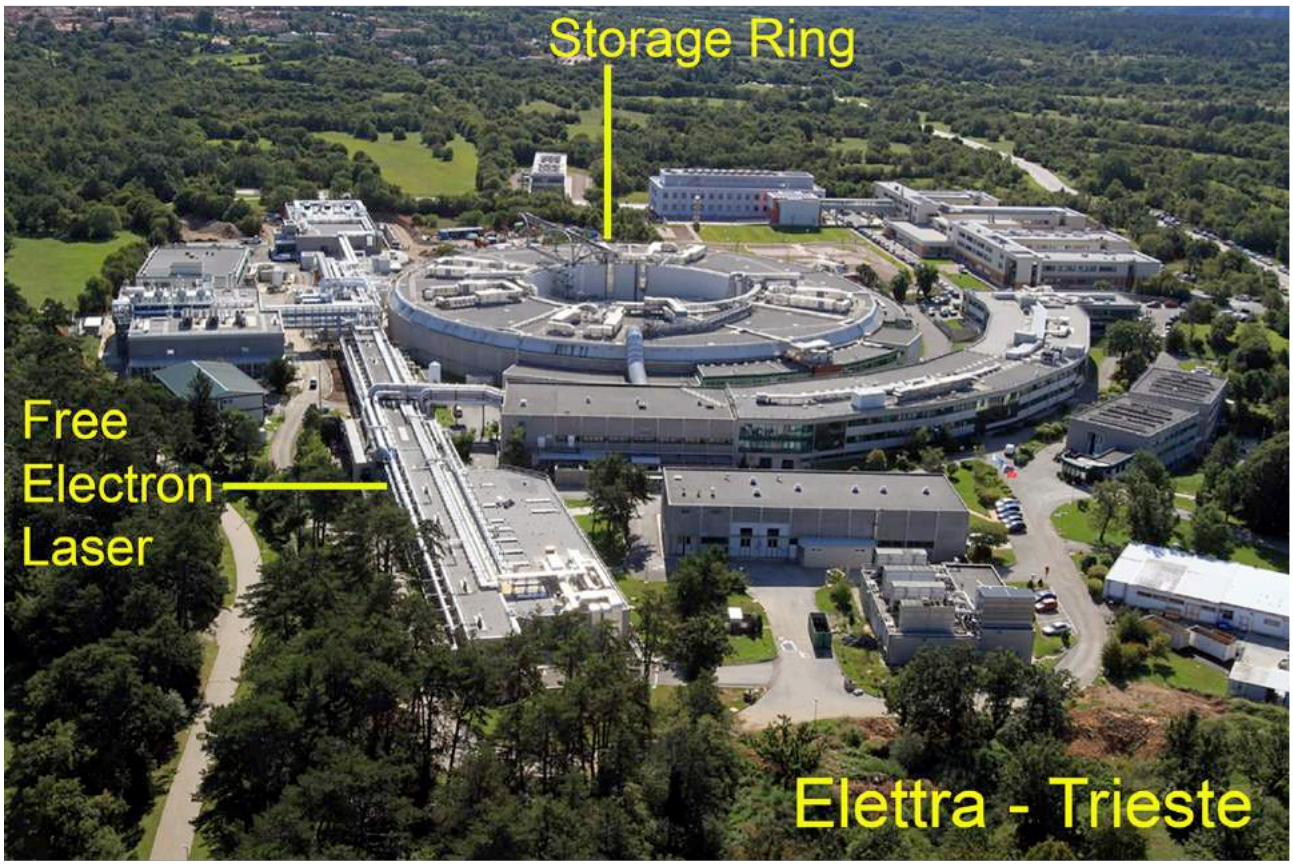

Fig. 1 – A modern synchrotron facility: Sincrotrone Trieste (Elettra). The donut-shaped building contains the storage ring Elettra itself, and the long straight structure houses the free electron laser system FERMI.

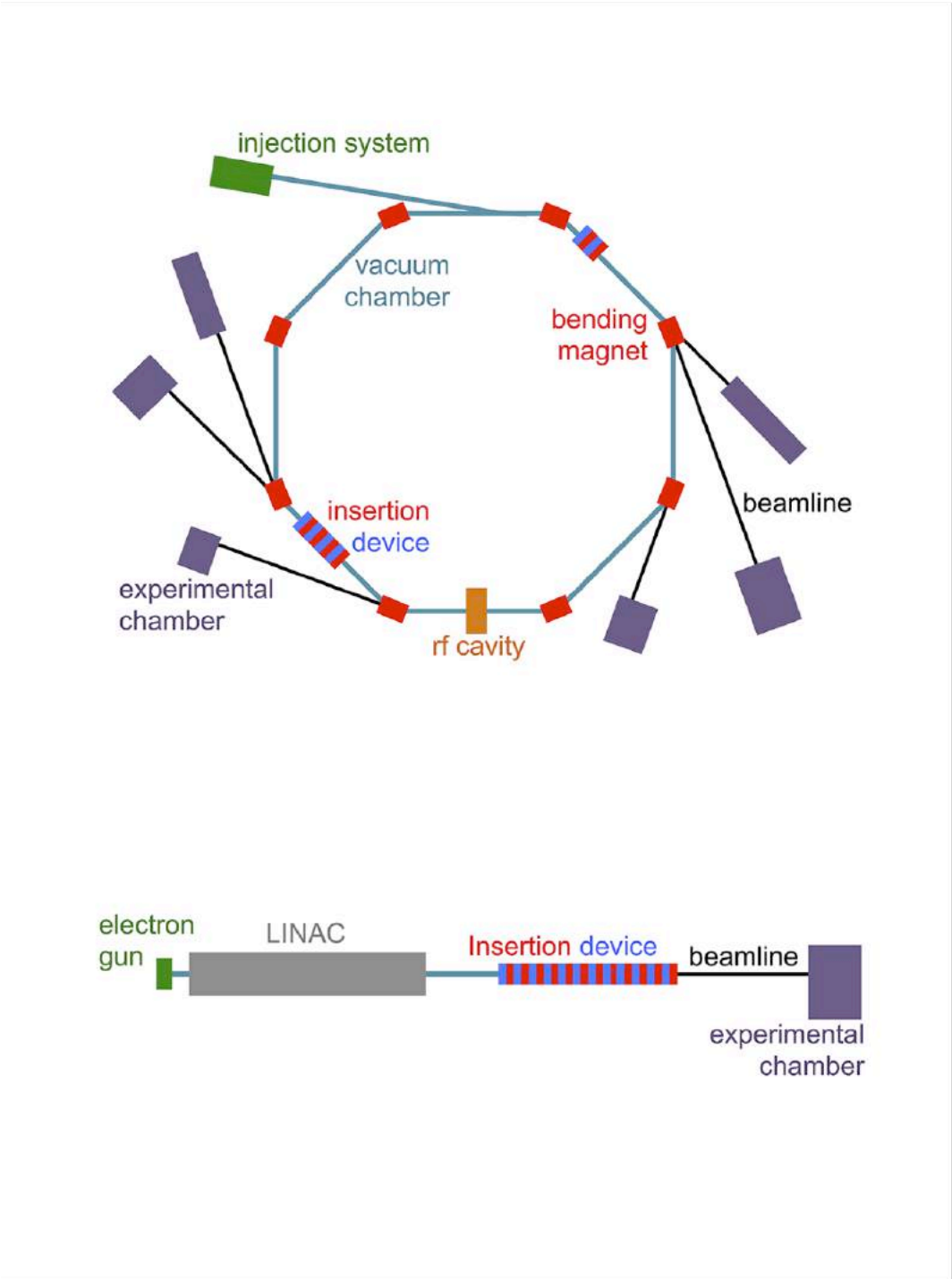

Fig. 2 – Top: simplified scheme of a storage ring source of synchrotron radiation with its main components. Bottom: layout of an x-ray free electron laser (x-FEL) based on a LINAC (linear accelerator). Both types of facilities include "insertion devices", periodic magnetic systems discussed later.

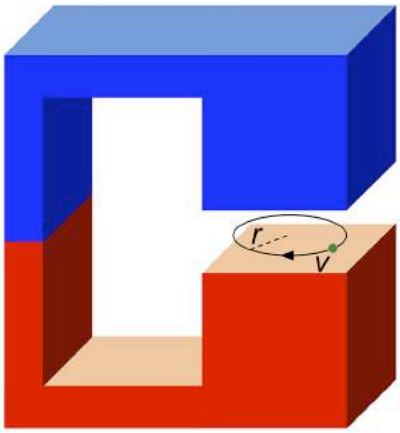

Fig. 3 – A simple source of synchrotron radiation: a dipole magnet that causes the horizontal "cyclotron motion" of an electron, whose centripetal acceleration produces electromagnetic waves. The text explains why the emitted wavelength is much shorter in the relativistic case than in the classical picture.

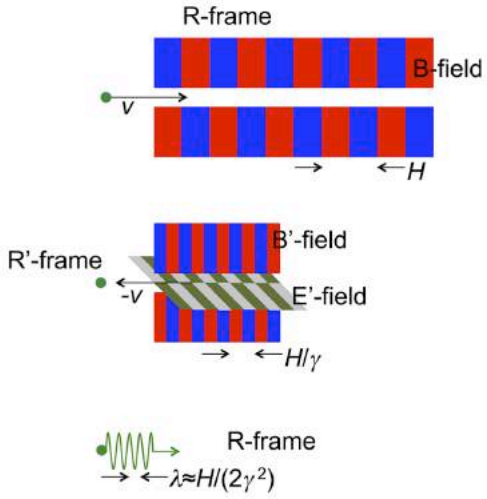

Fig. 4 - Another type of synchrotron source, an "undulator", consisting of a periodic series of magnets. Top: in the laboratory reference frame R, the undulator period is H and an electron moves towards it at a speed $v \approx c$. Middle: seen in the inertial reference frame R', which has the same longitudinal speed as the electron, the undulator moves at nearly the speed of light and its period shrinks to H/γ because of the Lorentz contraction; furthermore, the undulator (transverse) B'-field is accompanied by a transverse E'-field of equal period, perpendicular to it. The combination of propagating, transverse magnetic and electric fields resembles an electromagnetic wave. The backscattering of this "wave" by the electron produces synchrotron radiation, whose wavelength in R' is H/γ. Bottom: detected in the R-frame, the wavelength is Doppler-shifted (longitudinally) by a factor $\approx 2\gamma$, becoming $\approx H/(2\gamma^2)$.

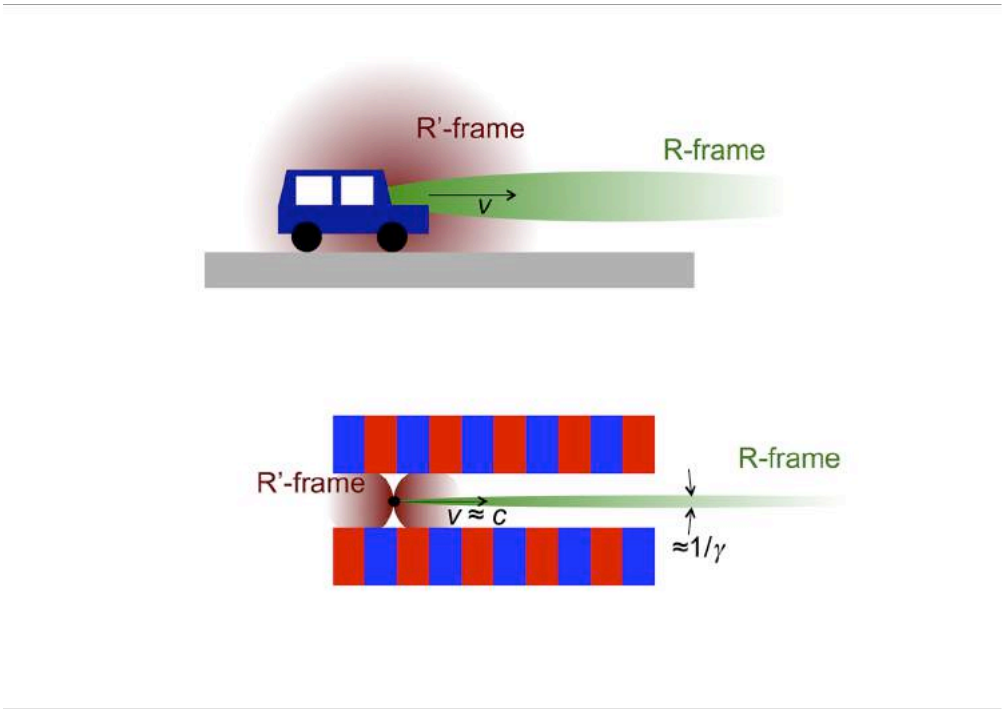

Fig. 5 – The angular collimation of synchrotron radiation is also a relativistic effect. Top: the emission of a conventional wave source such as a car horn, nearly isotropic in the R'-frame of the moving car, is "projected forward" when detected in the (road) R-frame. Bottom: for a fast-moving electron that emits synchrotron radiation, relativity makes this effect extreme, confining the emission in R to a very small angular range $\approx 1/\gamma$.

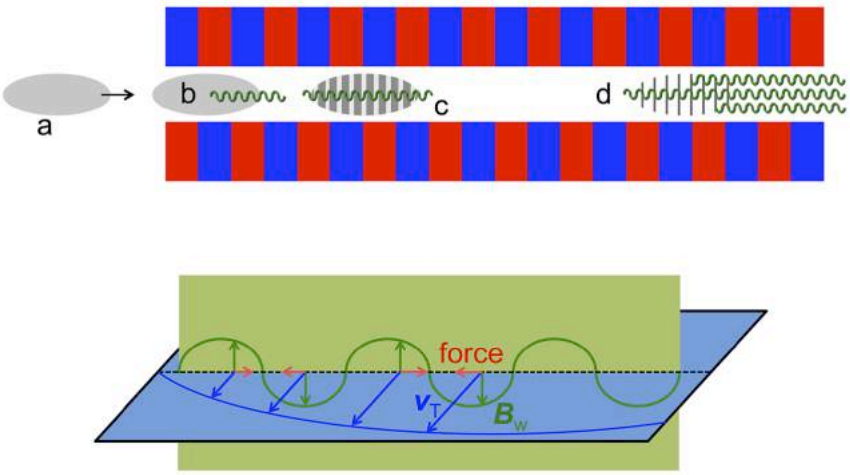

Fig. 6 – Schematic mechanism of a free electron laser (FEL). Top: A relativistic electron bunch approaches (a) and then enters (b) an insertion device, where its electrons start emitting waves. Then, the bunch and the waves travel together (c), and their interaction progressively confines the electrons to periodic "slices" (microbunches), with period equal to the wavelength. Next, (d) the microbunched electrons emit in a correlated way, amplifying the initial wave. Bottom: a detailed analysis shows that the transverse velocity $\boldsymbol{v}_T$ of the electrons and the magnetic B-field of the wave, $\boldsymbol{B}_w$, cause Lorentz forces that accumulate the electrons at every other wave node, explain why the "slice" period is one wavelength.

Radiation from Electrons in a Synchrotron

F. R. ELDER, A. M. GUREWITSCH, R. V. LANGMUIR,
AND H. C. POLLOCK
Research Laboratory, General Electric Company,
Schenectady, New York
May 7, 1947

HIGH energy electrons which are subjected to large accelerations normal to their velocity should radiate electromagnetic energy.[1–4] The radiation from electrons in a betatron or synchrotron should be emitted in a narrow cone tangent to the electron orbit, and its spectrum should extend into the visible region. This radiation has now been observed visually in the General Electric 70-Mev synchrotron.[5] This machine has an electron orbit radius of 29.3 cm and a peak magnetic field of 8100 gausses. The radiation is seen as a small spot of brilliant white light by an observer looking into the vacuum tube tangent to the orbit and toward the approaching electrons. The light is quite bright when the x-ray output of the machine at 70 Mev is 50 roentgens per minute at one meter from the target and can still be observed in daylight at outputs as low as 0.1 roentgen.

The synchrotron x-ray beam is obtained by turning off the r-f accelerating resonator and permitting subsequent changes in the field of the magnet to change the electron orbit radius so as to contract or expand the beam to suitable targets. If the electrons are contracted to a target at successively higher energies, the intensity of the light radiation is observed to increase rapidly with electron energy. If, however, the electrons are kept in the beam past the

Fig. 7 – Publication [16] by Herb Pollock's team of the first experimental observation of synchrotron radiation at GE, in 1947.

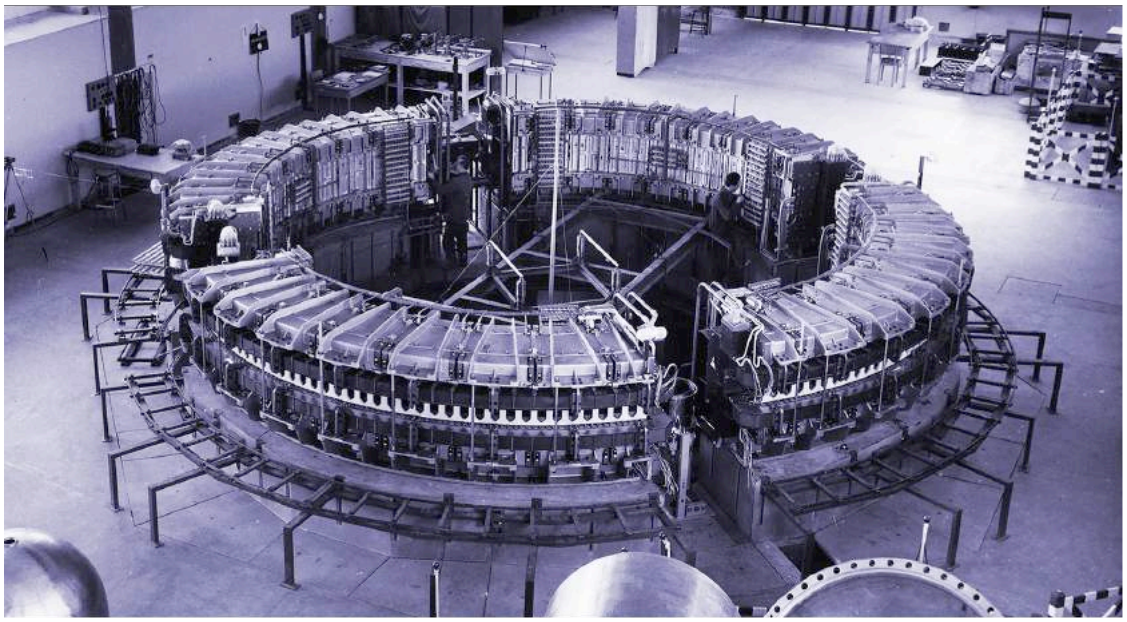

Fig. 8 – The Frascati 1.1 GeV electron synchrotron, constructed under the direction of Giorgio Salvini. This accelerator was used for the first sustained synchrotron radiation program in Italy, led by Gianfranco Chiarotti. Picture from http://w3.lnf.infn.it/synchrotron/?lang=en; copyright: INFN.

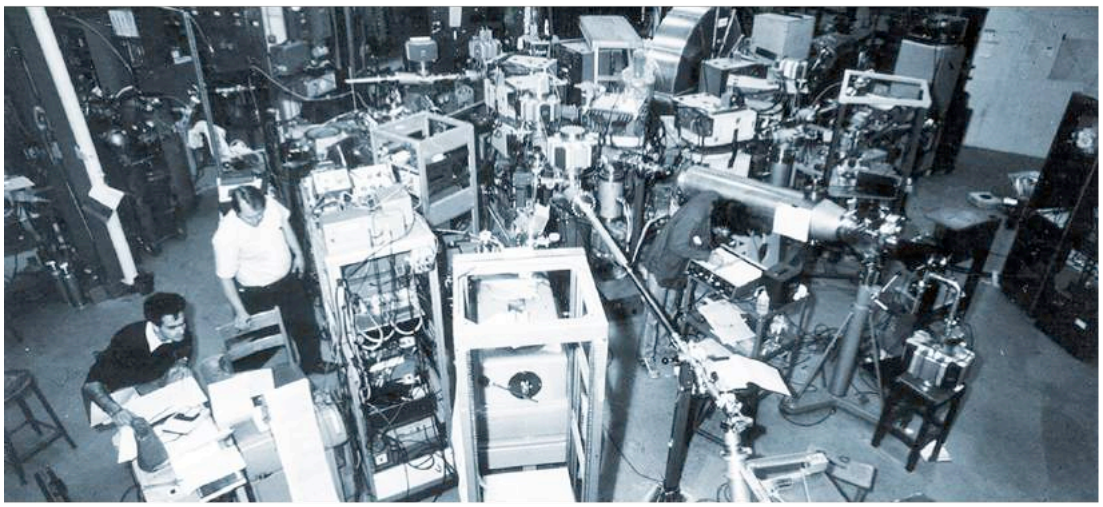

Fig. 9 – The 240 MeV storage ring Tantalus of the University of Wisconsin was the first dedicated synchrotron radiation source in the world [18-22]. On the left, two early users: Mario Piacentini (left) and Cliff Olson. Note the small size: the ring diameter was only 3 m. Image from http://invention.si.edu/tantalus-synchrotron-radiation-source, copyright 2017 Smithsonian Institution.

Fig. 10 – Artist portrait of Ednor M. Rowe, leader of the Tantalus project and founder of the Wisconsin Synchrotron Radiation Center (SRC) [18-22]. His pioneering intuition played a key role in the birth of synchrotron radiation.

Fig. 11 – Top: an historical picture, the celebrations at Tantalus after the first synchrotron radiation experiment with a dedicated source, performed by Helmuth Fritzsche's team on CdS [18-22]. We see in the picture, from left to right: Ulrich Gerhardt (of Fritzsche's group), the Tantalus staff members John Budden, Darrell Klimke, Roger Otte, and Dick Fasking, then Gary Rubloff (also of Fritsche's group), Roger Bartlett and Gordon Lassahn. Shortly afterwards, experimental results were also obtained on Tantalus by Fred Brown's and Dave Lynch's teams. Bottom: the Tantalus building, where the event took place. Pictures from [18].

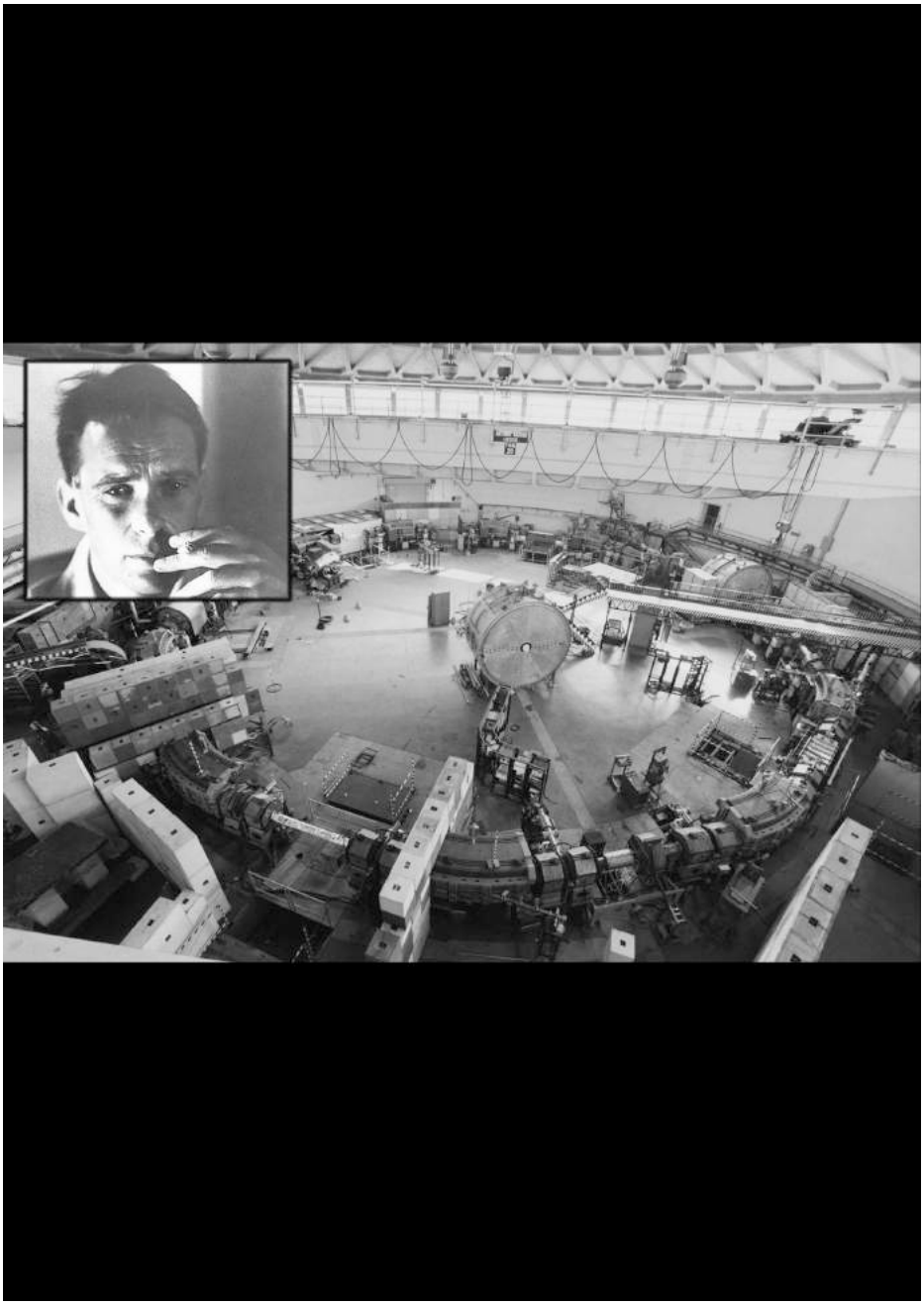

Fig. 12 – Bruno Touschek, pioneer and conceptual leader of the storage ring program in Frascati, with the Adone collider in the background [32,33]. The Adone picture is from http://w3.lnf.infn.it/adone/?lang=en; copyright: INFN.

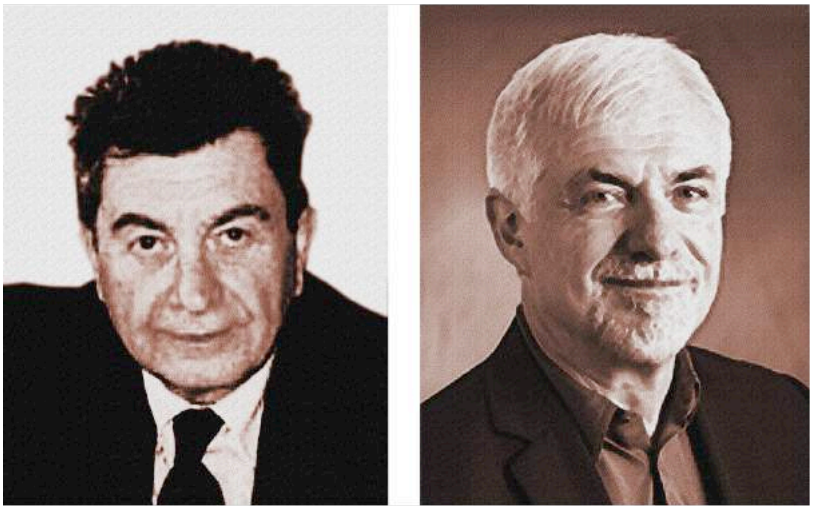

Fig. 13 – Artist portraits of Franco Bassani (left), director of the Frascati PULS project, and Franco Cerrina, one of the most outstanding alumni of the Frascati synchrotron radiation programs.

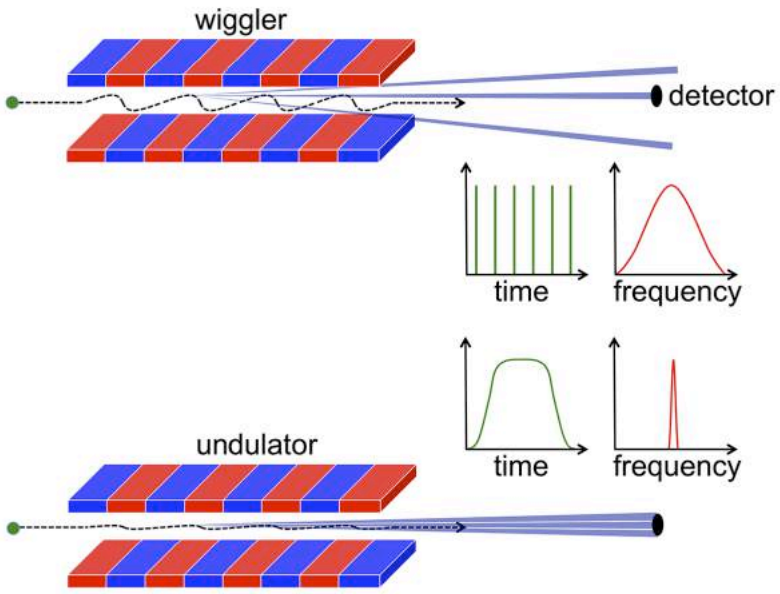

Fig. 14 – Differences between a wiggler (top) and an undulator (bottom). The wiggler magnetic field intensity is strong and produces (relatively) large transverse electron oscillations (exaggerated here for clarity). As a consequence, the narrow emitted cone of radiation does not continuously illuminate the (point-like) detector, which detects a series of pulses. Due to the Fourier transform properties, this corresponds to broad frequency and wavelength bandwidths. The weak B-field of the undulator produces instead a single, long pulse and narrower bandwidths.

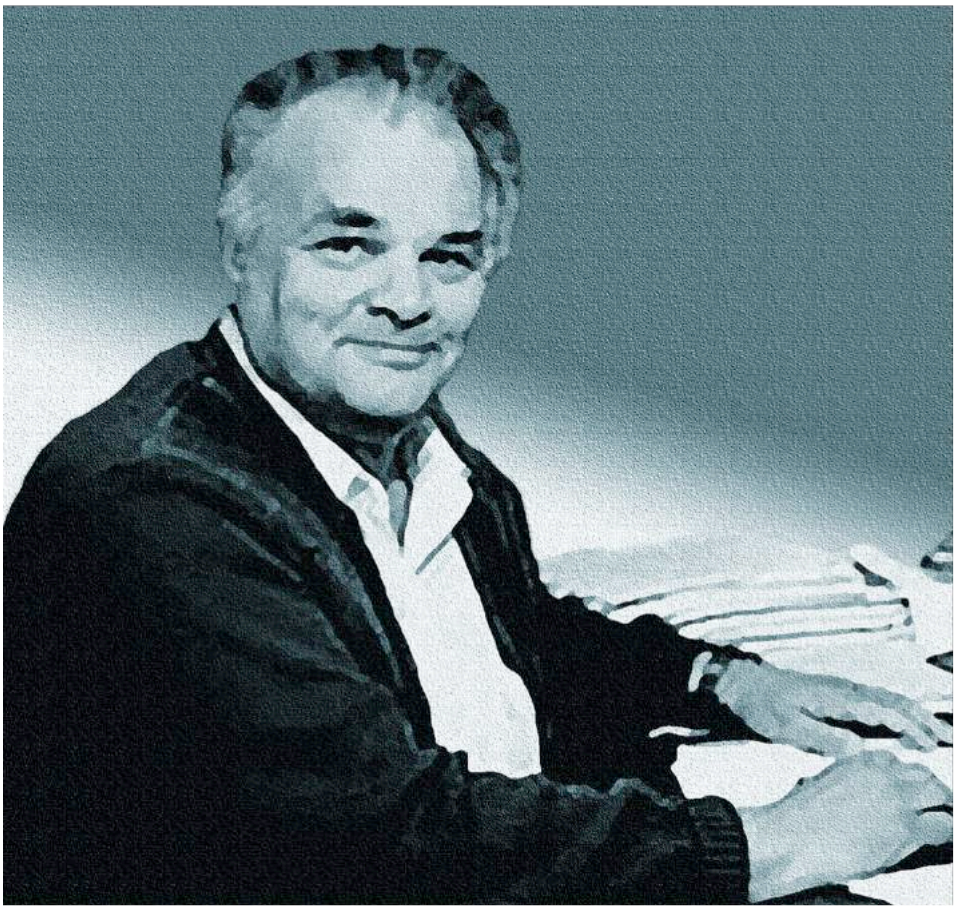

Fig. 15 – Artist portrait of Klaus Halbach, eminent father of the insertion devices that characterized the "third generation" of synchrotron sources [13].

Fig. 16 – The Swiss Light Source (SLS), one of the third-generation synchrotron facilities. Copyright: EPFL; courtesy of Joel Mesot.

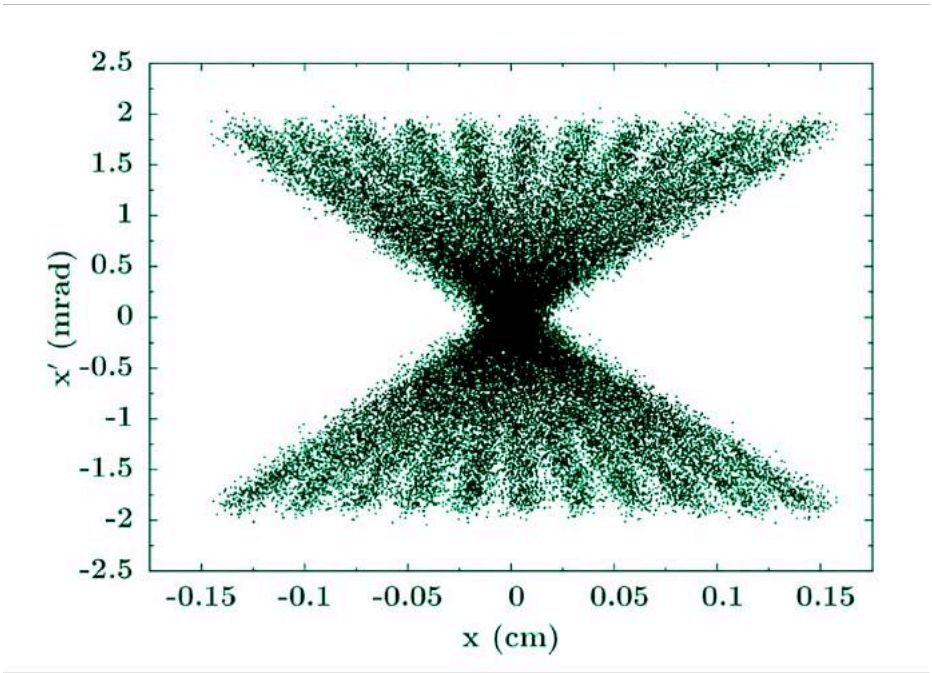

Fig. 17 – Example of results of the "Shadow" software, the world standard for beamline design, developed under the leadership of Franco Cerrina [35]. Image from [35]; copyright: International Union of Crystallography.

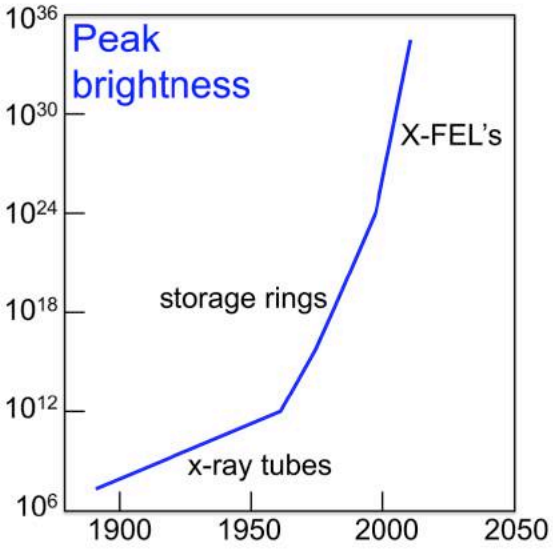

Fig. 18 – The historical progress of the brightness (or brilliance) of x-ray sources. The units here are photons/mm^2/s/mrad^2, for a 0.1% spectral bandwidth. Note the very large range of the logarithmic vertical scale.

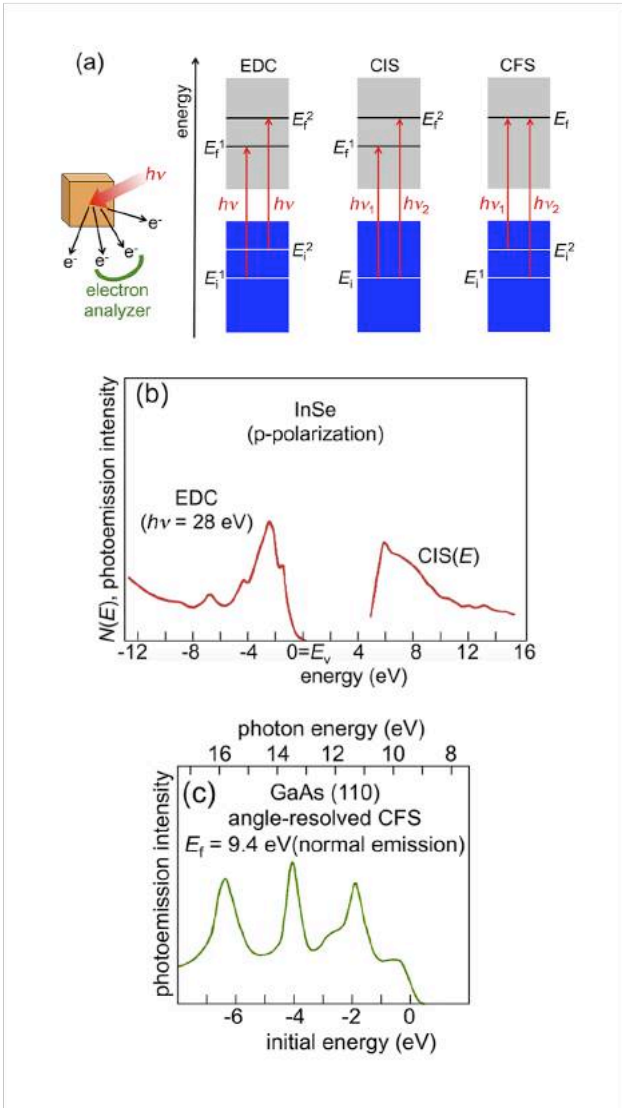

Fig. 19 – (a) three modes [43-45] of photoemission spectroscopy using synchrotron radiation. In the conventional EDC (Energy Distribution Curve) mode, the photoemission intensity is measured as a function of the photoelectron energy for a constant photon energy *hv*. The EDC's reflect the initial energy distribution of the electrons in the sample, but are affected by transition probability effects, since different final-state energies (*e.g.*, E_f^1 and E_f^2) correspond to different initial-state energies (E_i^1 and E_i^2). In the CIS (Constant Initial State) mode, *hv* and the photoelectron energy are simultaneously scanned while keeping constant their difference: this corresponds to a constant initial-state energy E_i, and the spectra reflect the density of unoccupied states. In the CFS (Constant Final State) mode, the photoelectron energy is kept constant while scanning *hv*: the spectra reflect the initial-state energy distribution as the EDC's -- but with more limited transition probability effects. (b) A combination of EDC and CIS results reveals the energy distribution both of the occupied (valence) states and the unoccupied (conduction) states in the layer compound InSe [48]. (c) Example of CSF spectrum [43].

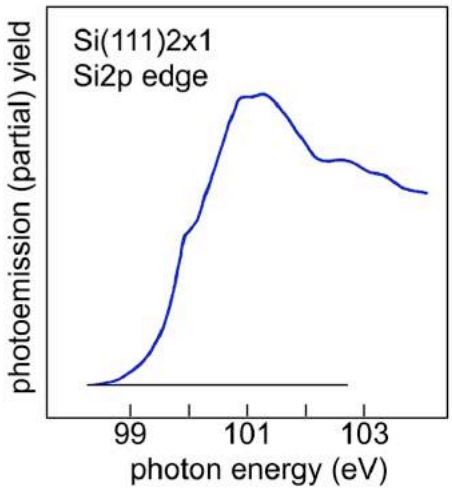

Fig. 20 – Early example of partial-yield (surface absorption) spectrum for an ultraclean Si(111)2×1 surface, in the spectral region of the Si2p edge [49].

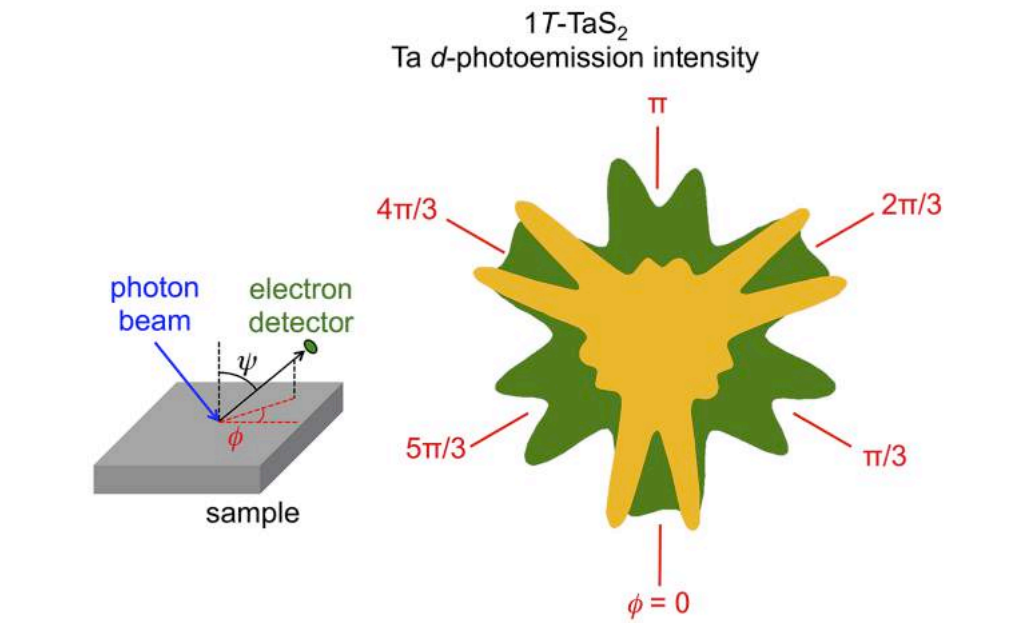

Fig. 21 – The dependence of the photoemission intensity on the emission angle clearly reflects the symmetry of the 1*T*-TaS_2 surface [50]. These patterns were taken by scanning the azimuthal angle ϕ (parallel to the emitting surface, as shown on the left-hand side) while keeping constant the angle ψ with respect to the surface normal. The two ϕ-patterns correspond to two different values of ψ. The information used for the figure was obtained from [50].

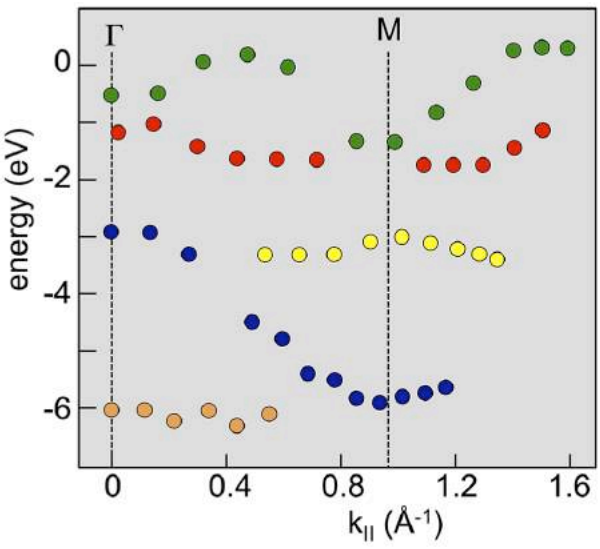

Fig. 22 – Early example of experimental "band structure mapping" by angle-resolved synchrotron radiation photoemission, performed for the layer compound GaSe [51]. The experimental results closely resembled the calculated band structure by Mike Schluter, and definitely proved the validity of the band mapping technique.

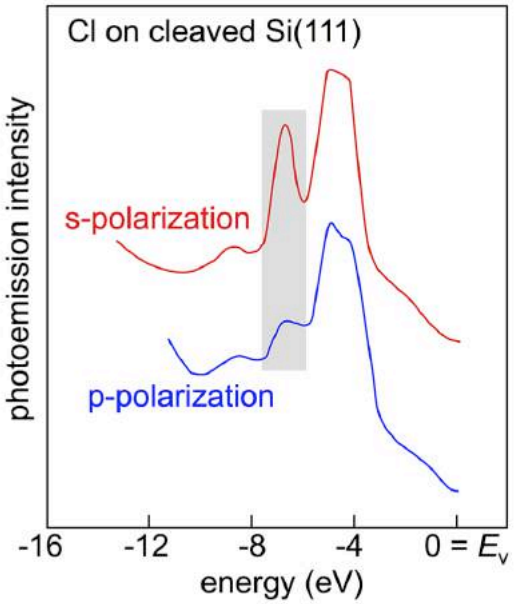

Fig. 23 – The linear polarization of synchrotron radiation reveals the effects of photon polarization in the photoemission spectra. In this early example, such effects (shaded area) identified the chemisorption geometry of Cl on cleaved Si(111) [52].

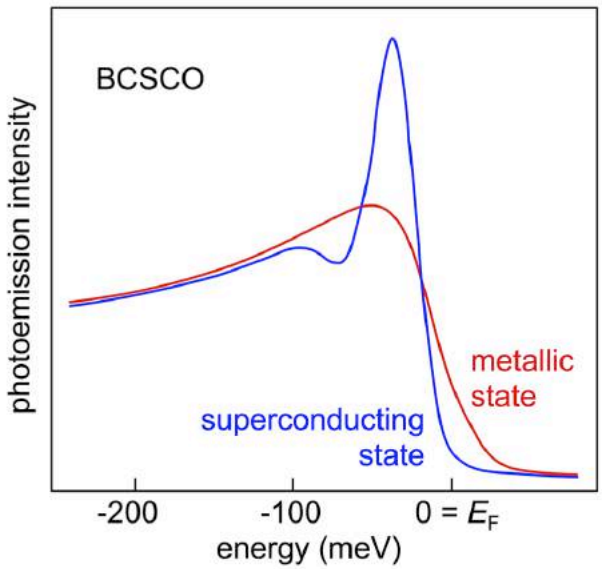

Fig. 24 – High-resolution synchrotron photoemission reveals the gap features of high-temperature superconductors. The leading edges of spectra taken by Yeukuang Hwu *et al.* in BCSCO [36], at temperatures above and below the superconducting transition, show the opening of the gap. And the superconducting-state spectrum also reveal other spectral features that were intensively explored in subsequent years.

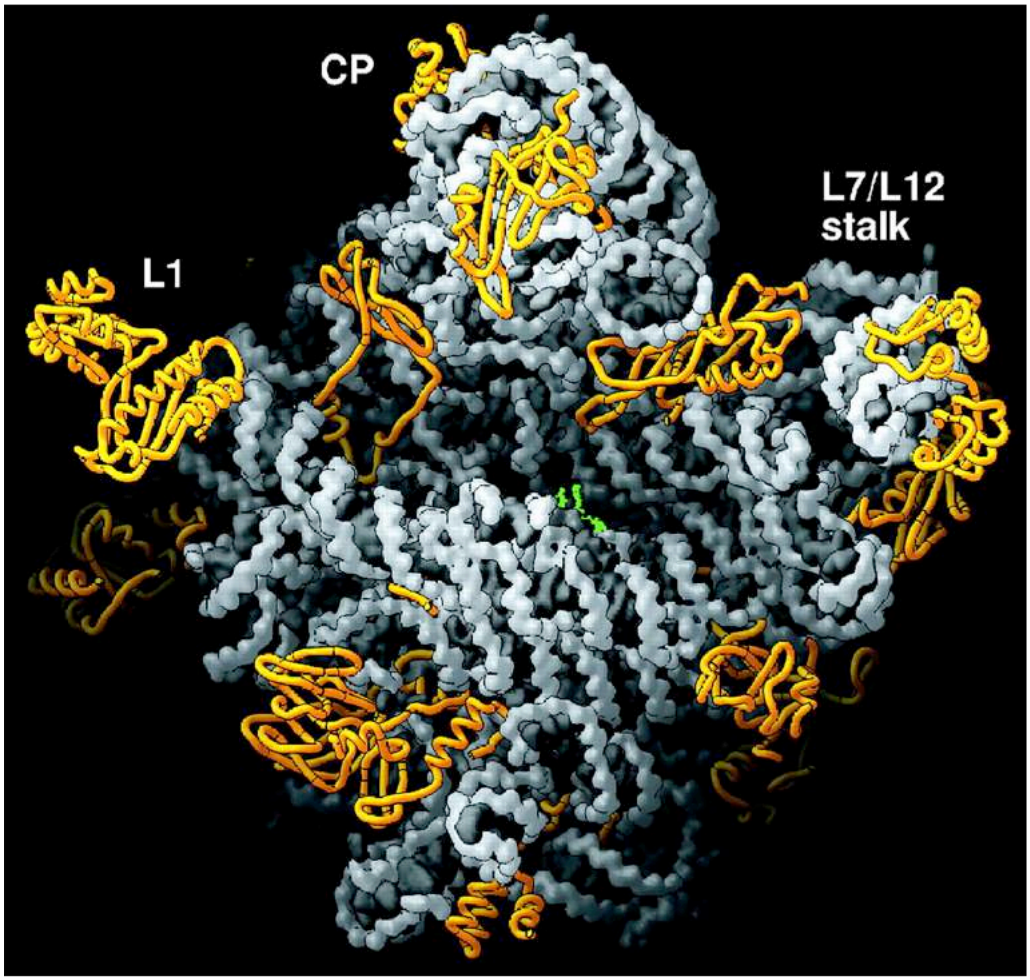

Fig. 25 – An example among many of crystallography with synchrotron radiation: the *Haloarcula marismortui* large ribosomal subunit in the rotated crown view [64]. The experiment was performed at the Brookhaven and Argonne facilities. Figure from [64], Copyright © 2000, The American Association for the Advancement of Science, reprinted by permission.

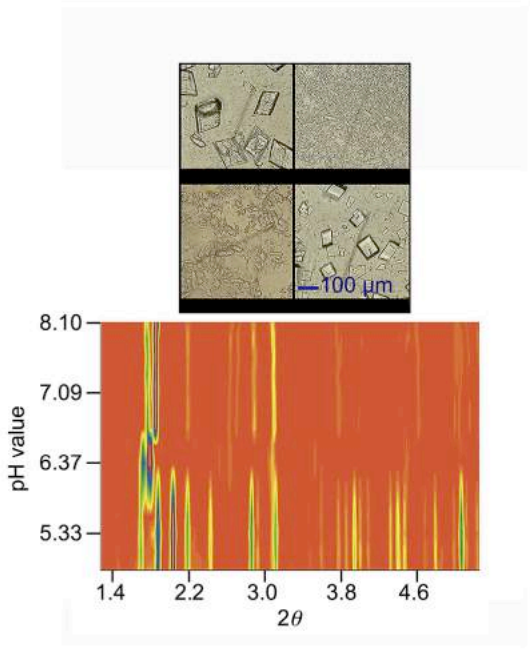

Fig. 26 – X-ray powder diffraction (XRPD) results from [67]. Top: the investigated polycrystalline samples: human insulin co-crystallized with 4-ethylresorcinol corresponding to pH values of 5.00 (upper left), 5.80 (upper right), 5.97 (lower left) and 7.37 (lower right). The data analysis [67] shows that each crystalline phase corresponds to a different symmetry. Bottom: color rendering of XRPD data for different pH values. Image from [67], copyright: International Union of Crystallography.

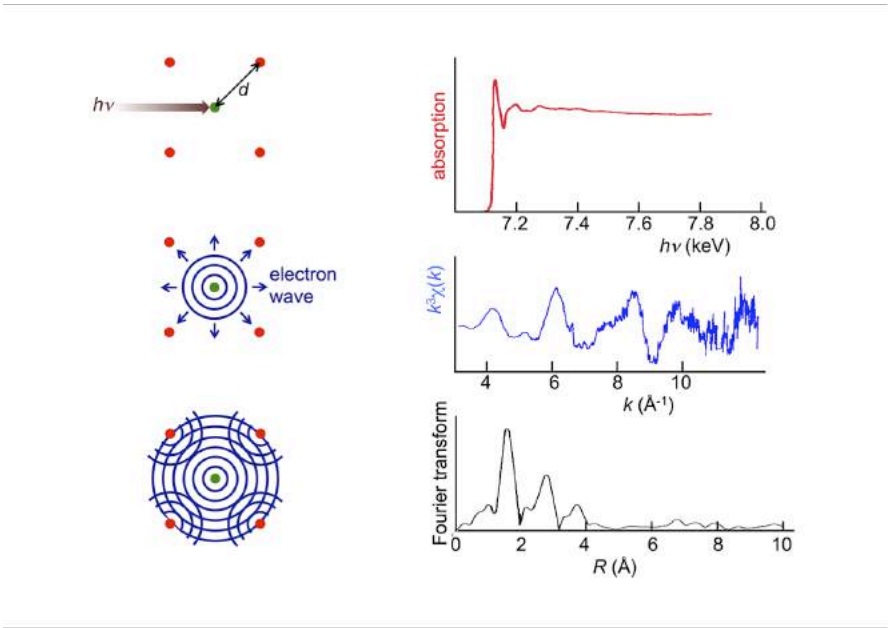

Fig. 27 – Left: simplified picture of the EXAFS mechanism. At the top left, an atom (green dot) of a given chemical element in a condensed matter system absorbs an x-ray photon *hν*. Immediately below, the excited electron wave propagates away from the central atom. Bottom left: the electron wave is partially backscattered by the (red) neighboring atoms at a distance *d*.. The interference of the outgoing and backscattered waves at the central site, depending on the electron wavelength and therefore on the photon energy, produces the EXAFS modulation of the absorption coefficient. Right: one of early examples of synchrotron EXAFS [71]. From top to bottom: the weak EXAFS modulation above the Fe K-edge of deoxygenated hemoglobin; the magnified modulation *vs.* the excited-electron k-vector magnitude; the Fourier transform of the previous curve, whose main peak reveals the distance *d*. Results from [71], copyright: Nature, reproduced by permission.

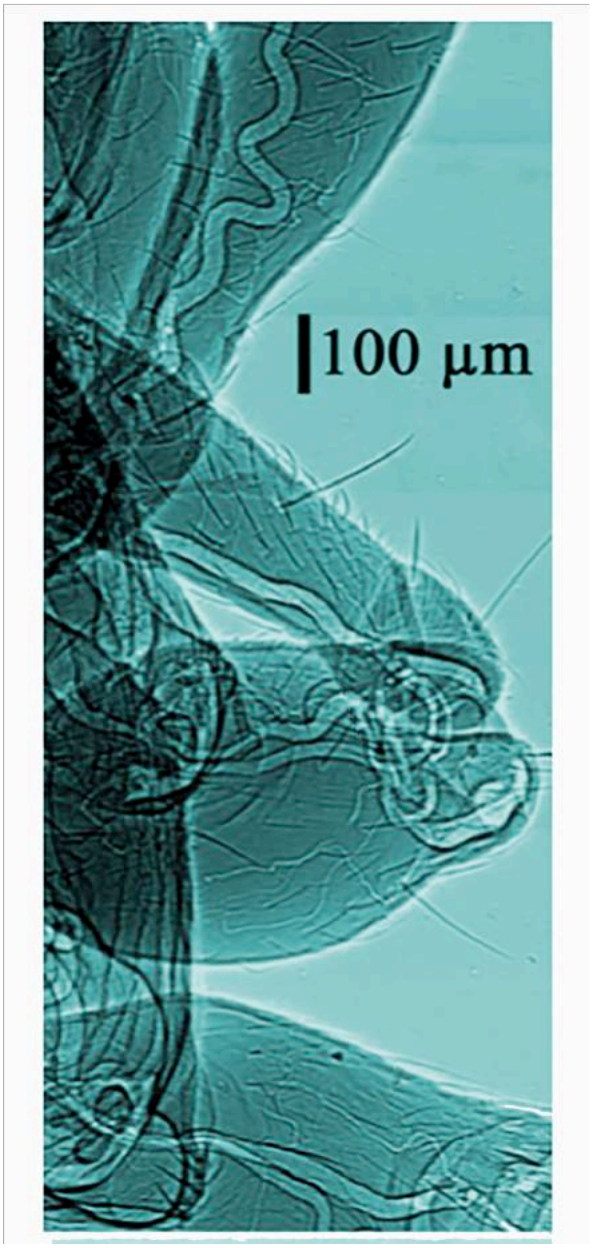

Fig. 28 – Example of phase contrast radiology made possible by the high spatial coherence of synchrotron radiation. Note the characteristic enhancement of the edges between different regions [73,81]. The specimen is a portion of the body of an ant.

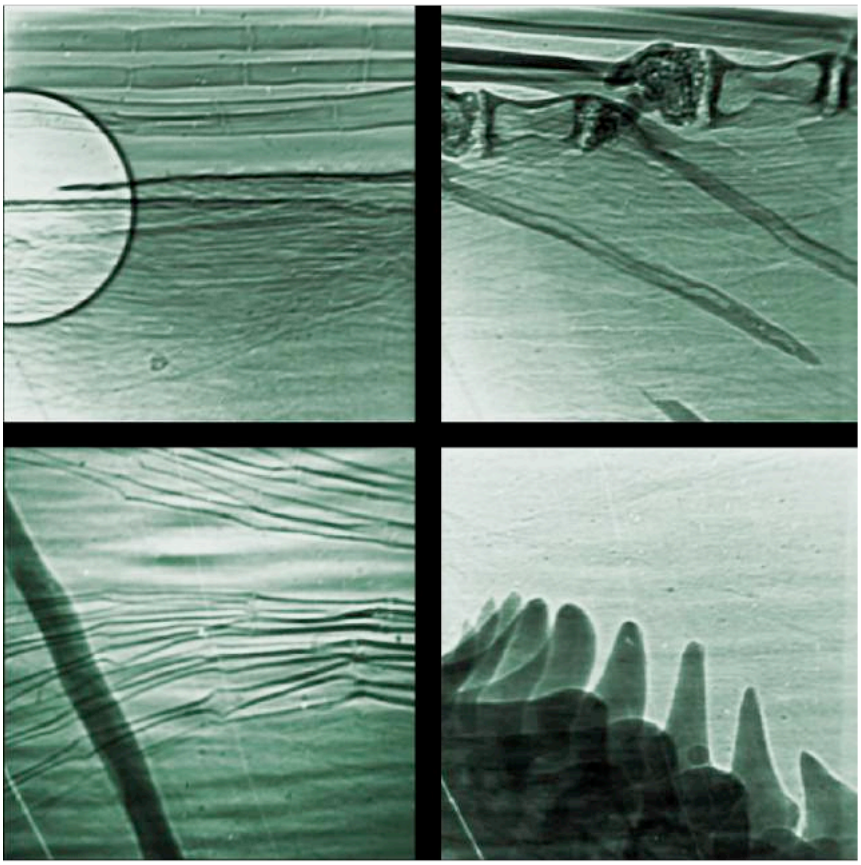

Fig. 29 – Another example of phase-contrast edge enhancement: images of different parts of a microscopic fish [81].

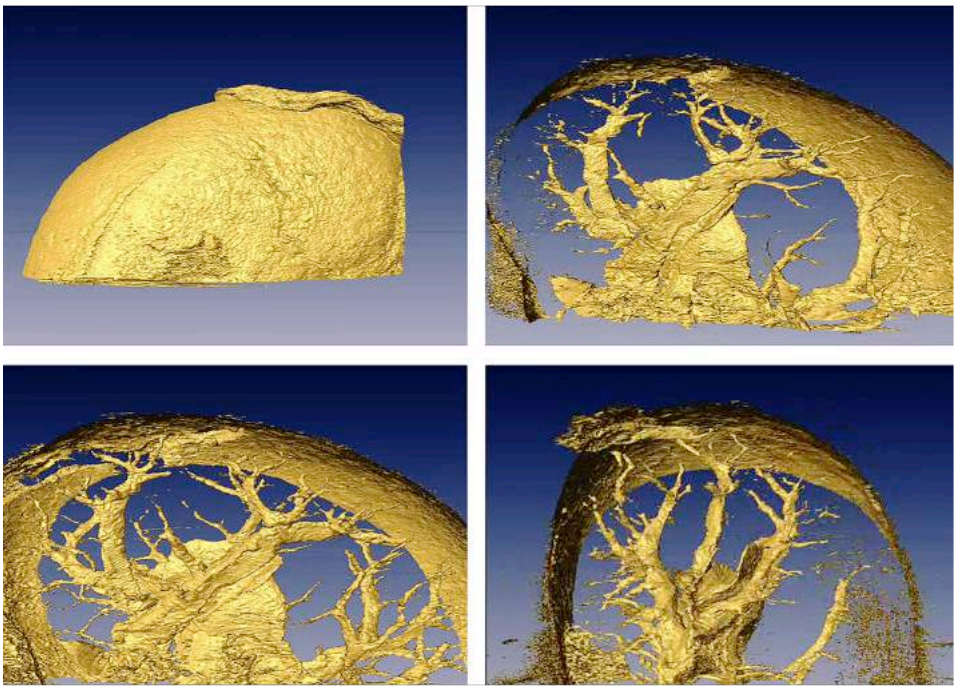

Fig. 30 – Tomographic (CAT) reconstruction images of a mouse kidney, obtained by computer-processing many phase-contrast projection radiographs, taken in different directions with constant angular spacing [85].

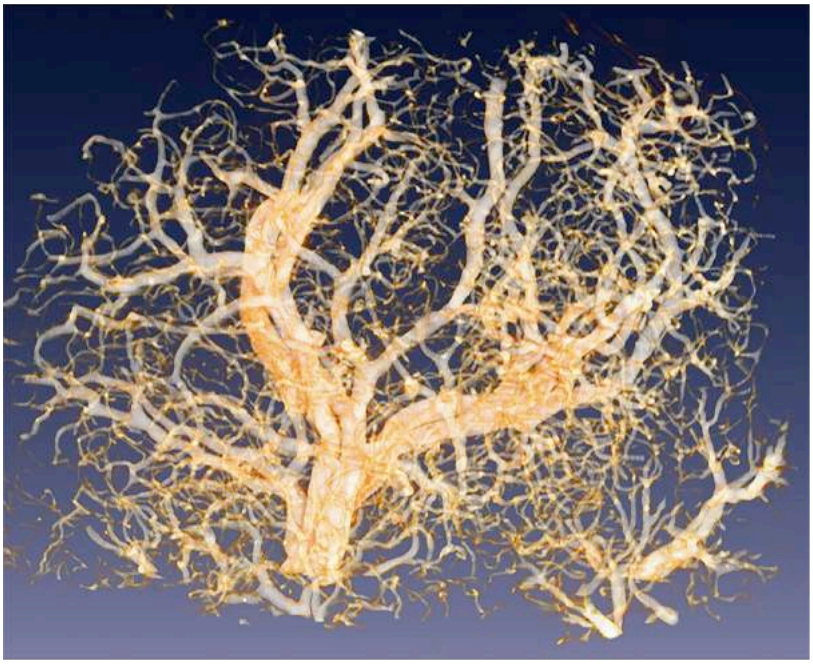

Fig. 31 – Another example of phase-contrast tomography: reconstructed image of the microvasculature accompanying the formation of a tumor (an ortopic pancreatic tumor genesis model). Data from [86].

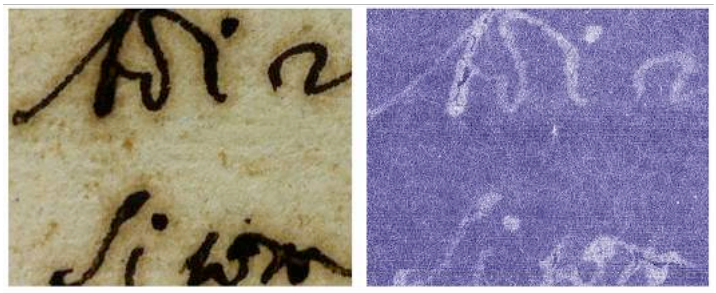

Fig. 32 – Synchrotron x-ray imaging is now used in previously unforeseen domains. Here, it allows the non-invasive detection of text in sealed ancient manuscripts [87,88], minimizing the risk of damage. Left: visible-light picture; right: the corresponding synchrotron radiographic image, showing handwritten letters -- thanks to the high absorption contrast produced by the ancient "iron gall" ink. In parallel, phase contrast reveals the morphological details of the substrate.

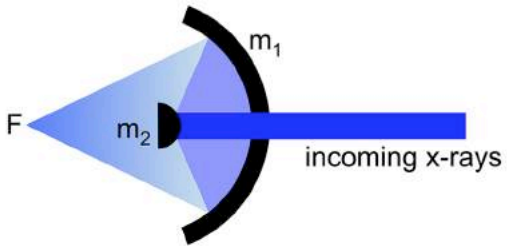

Fig. 33 – Schematic side view of a Schwarzschild objective [89]. The incoming x-ray beam passes through an aperture in the concave mirror m_1 and reaches the convex mirror m_2. Then, m_2 reflects the x-rays to m_1, which then concentrates the radiation to the focal point F. Both mirrors use reflections at near-normal incidence, which is very weak for x-rays. To enhance the reflectivity, the mirror surfaces were coated with multilayer films – not an easy task on a curved surface [89].

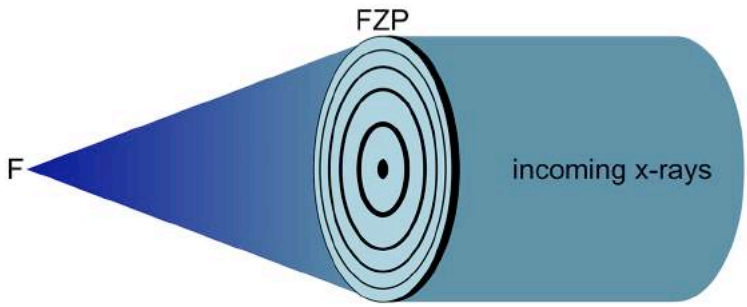

Fig. 34 – Scheme of a Fresnel zone plate [90] objective, the combination of circular, concentric transmitting and absorbing structures. The interference of the waves passing through the transmitting zones concentrates them to the focal point F.

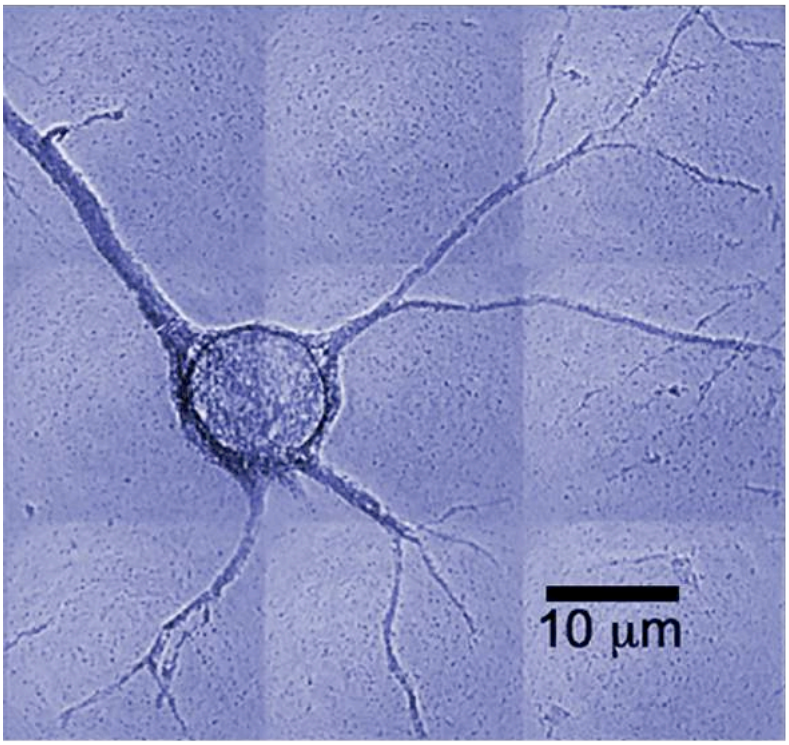

Fig. 35 – A benchmark result made possible by the progress in FZP fabrication: radiograph of an individual neuron cell. Data from [91].

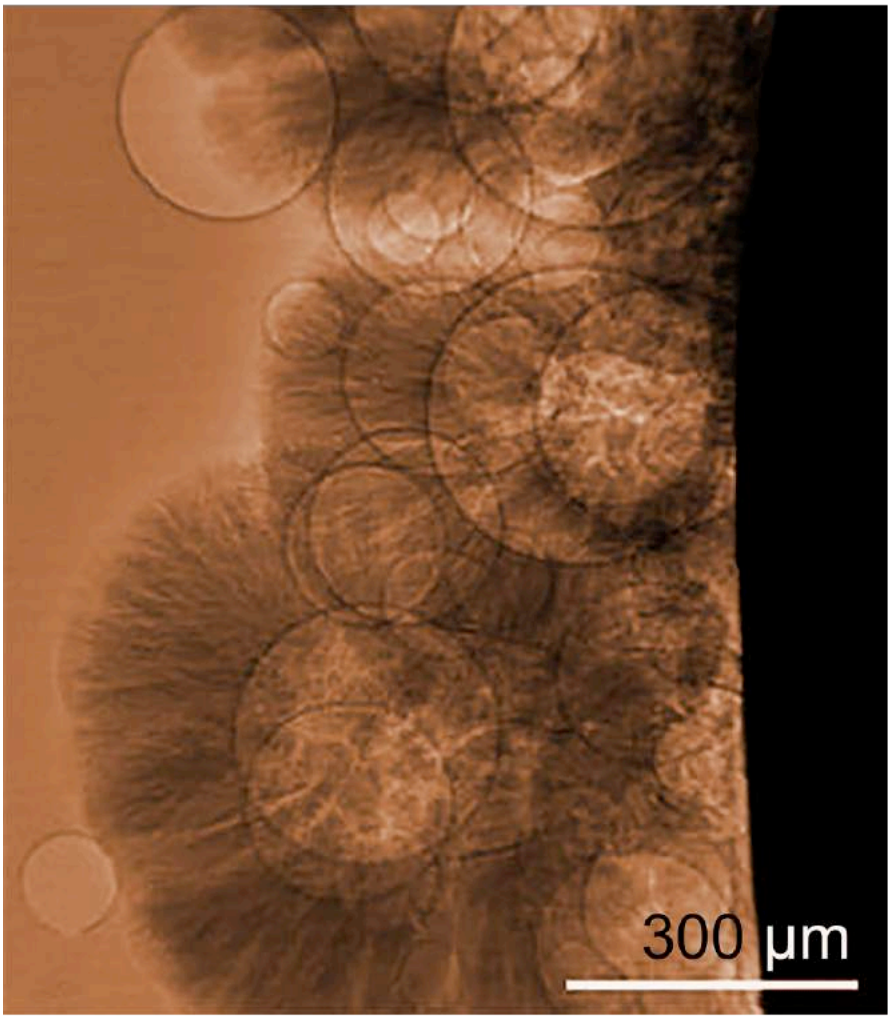

Fig. 36 – Fast data taking in phase contrast microradiology allowed observing in real time the electrodeposition of a zinc overlayer on a Zn substrate (the dark area on the right). This snapshot, taken from a movie, reveals an almost incredible phenomenon: the growth of zinc on the gas bubbles that are formed near the surface and then quickly disappear. Data from [93].

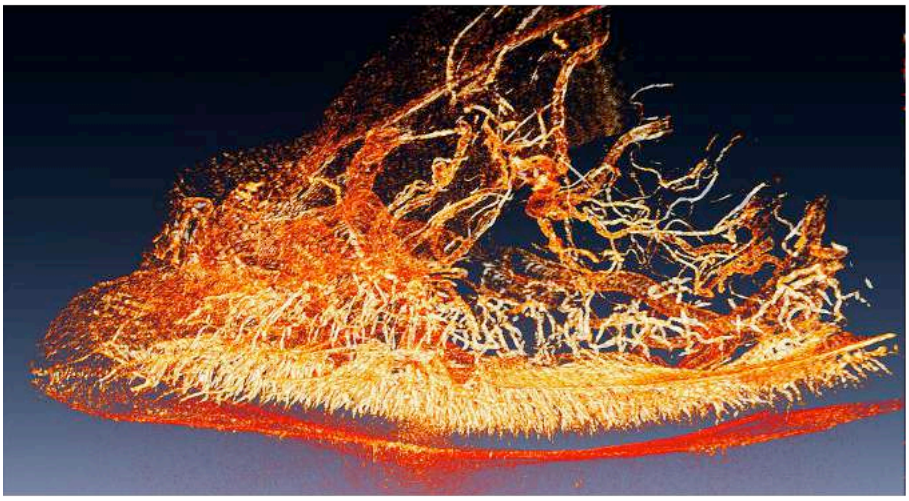

Fig. 37 – Tomographic reconstruction and phase contrast reveal all the microscopic details of the lantern system of a firefly, clarifying its fascinating light-emission mechanism. Data from [94].

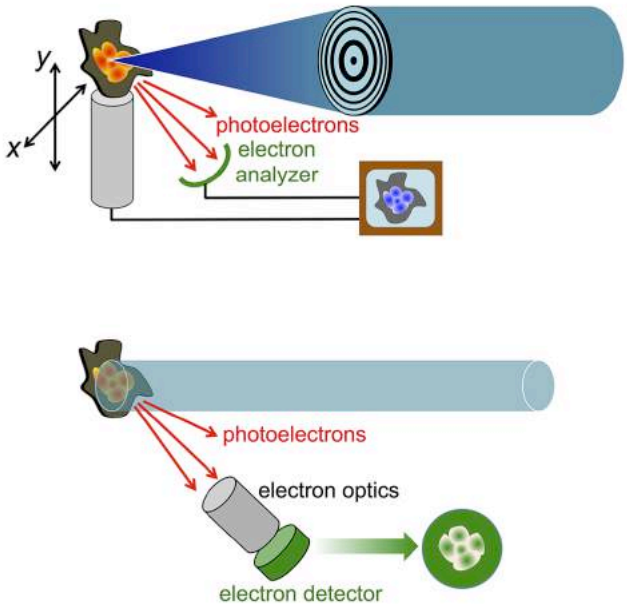

Fig. 38 – Two complementary approaches to photoemission spectromicroscopy. Top: the x-ray beam is focused into a small specimen spot by a lens, e.g., a FZP. An electron analyzer then detects the emitted photoelectrons. The specimen position can be scanned in the transverse *xy* plan, producing two-dimensional photoemitted-intensity "images". If the photoelectron energy corresponds to a core level of a specific chemical element, this yields "microchemical images" of its microscopic distribution [94]. Bottom: the lateral resolution here is not achieved by x-ray focusing but by processing the photoelectrons with an electron optics system. This is the foundation of PEEM techniques [95,96].

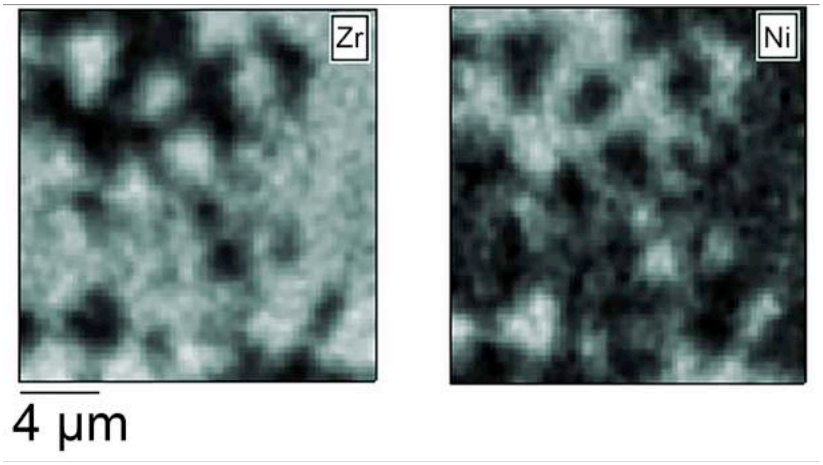

Fig. 39 – Example of "microchemical pictures" [95] by the approach in the top part of Fig. 38. Images of the specimen at the Zr3d and Ni2p photoelectron energies reflect the spatial distribution of the corresponding elements. Picture from [95], copyright: American Chemical Society, reproduced by permission.

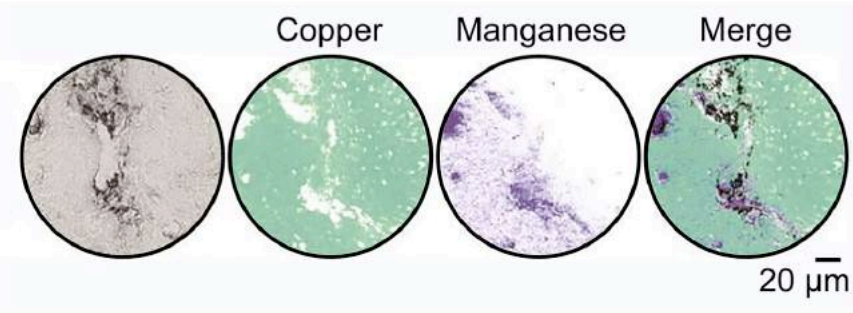

Fig. 40 – Example of microchemical images obtained with PEEM spectromicroscopy: trace elements (top labels) in a brain specimen (left picture) affected by transmissible spongiforme encephalopathy (TSE). Image reproduced from Johnson C. J. *et al.* [98] (open access).

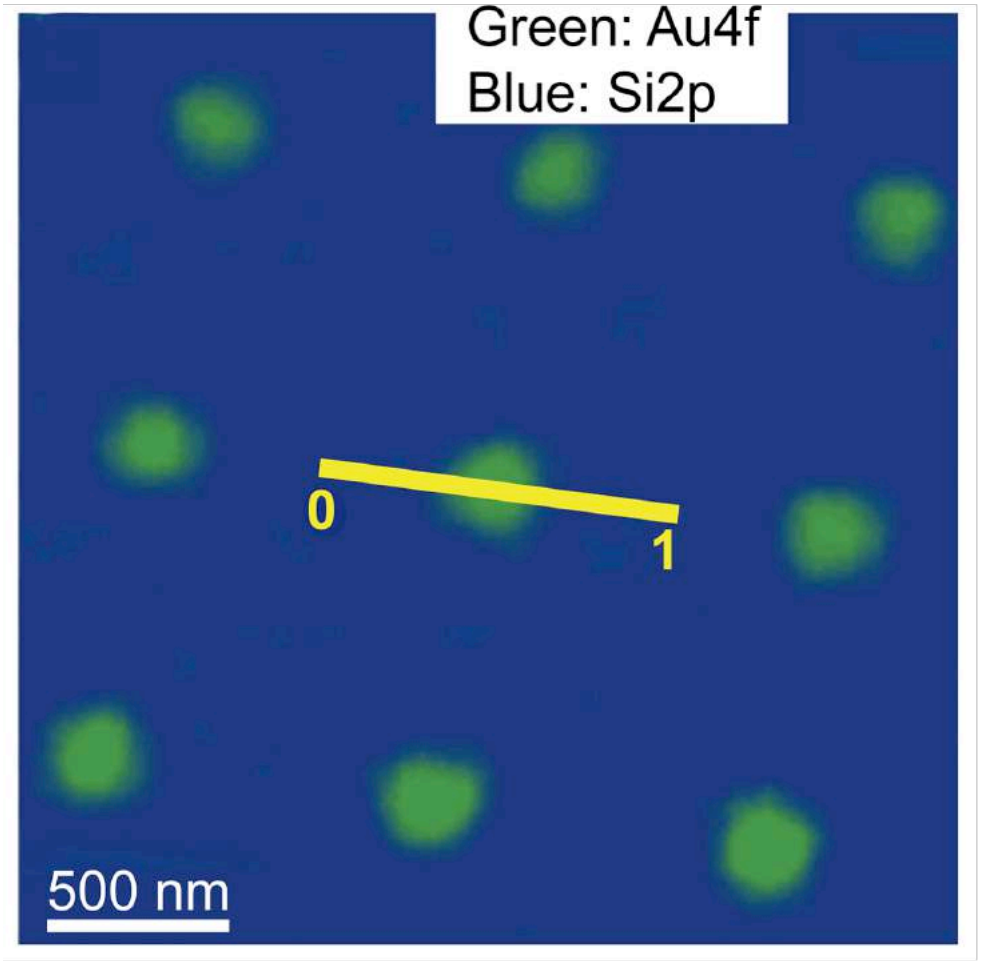

Fig. 41 – A nice example [99] illustrating the spectacular advances of PEEM techniques during the years 2000's: composite micrograph combining the Au4f and the Si2p energy-filtered images from an Au-patterned Si(001) sample (the yellow reference line is explained in [99].

Fig. 42 – Franco Cerrina's humorous version of a beamline alignment operation in Frascati. The comments in Italian are (from left to right): "Ehi, Massimo!"; "A bit higher… no… on the right… up, Luciano"; "We are accurately aligning the beamlines, and…"

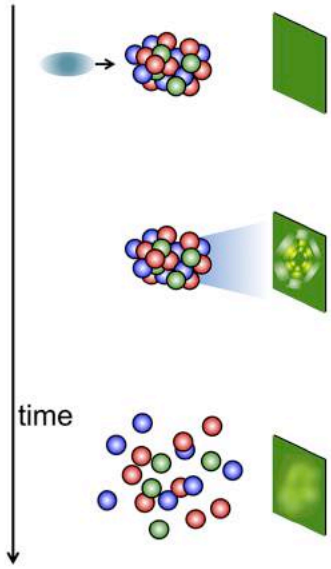

Fig. 43 - Scheme of one-shot structure determination with an x-FEL [107-109]. From top to bottom: (i) an x-FEL pulse hits the specimen, and (ii) produces a transient diffraction pattern, but then rapidly (iii) causes the destruction of the specimen and of the pattern. However, if the pulse is short enough one can extrapolate from the transient pattern the structure of the undamaged system.

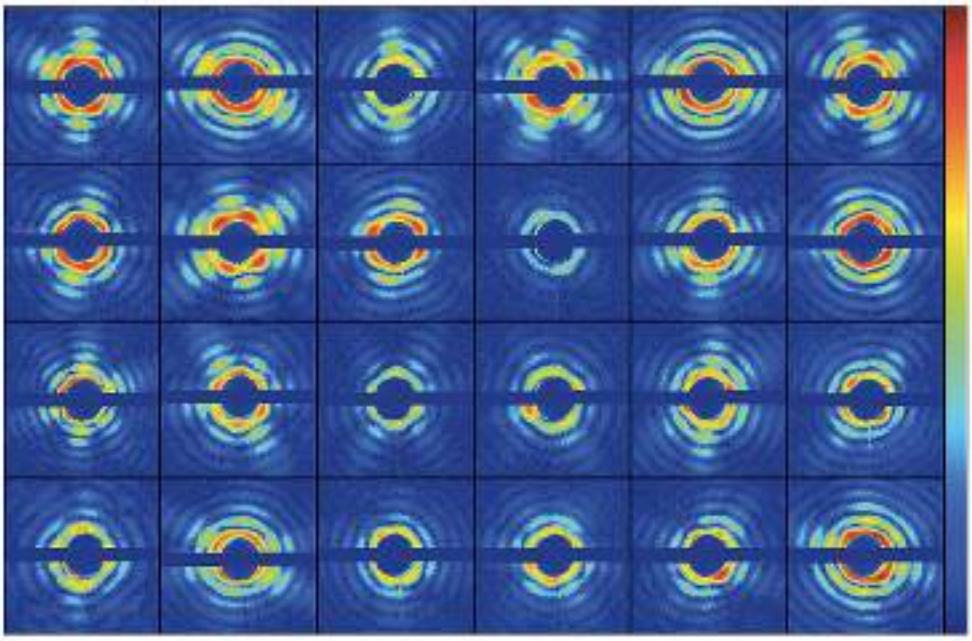

Fig. 44 – A recent example of one-shot structure determination with an x-FEL [111]: a series of individual diffraction patterns of Acanthamoeba polyphaga mimivirus particles taken at LCLS [111]. Copyright: American Physical Society, reproduced by permission.

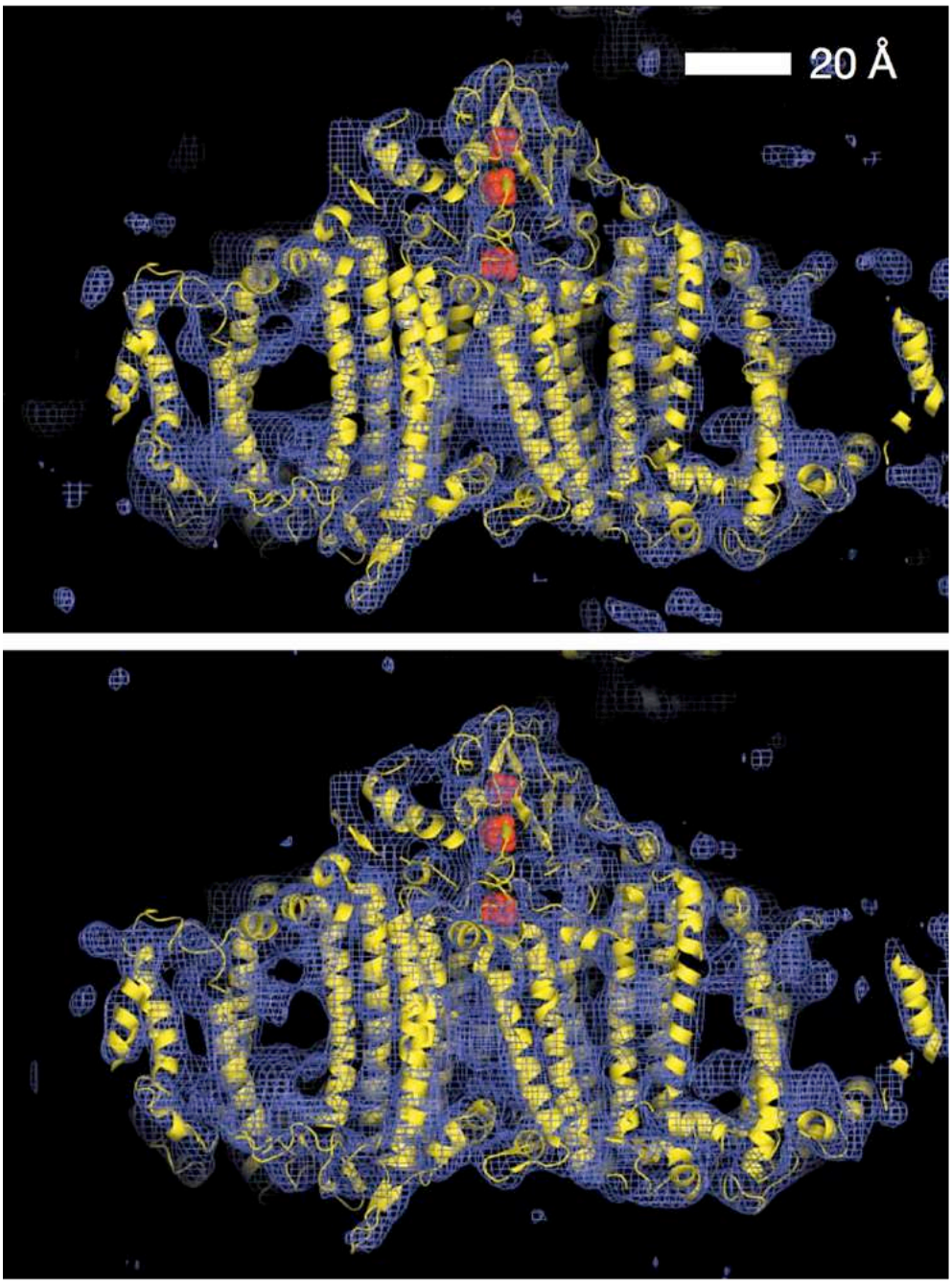

Fig. 45 – Another example of one-shot x-FEL structure determination [109]. The specimen is a membrane protein complex (1-MDa molecular mass, 36 proteins, 381 cofactors), a bio-solar energy conversion agent in oxygenic photosynthesis. Top: electron density map at 1.0 σ (purple mesh), derived from diffraction data produced by 70 femtosecond x-FEL pulses. Bottom: the equivalent map derived from a conventional synchrotron diffraction experiment (truncated at 8.5 Å resolution). The yellow parts correspond to the refined model of [109]. Image from [109], copyright: Nature, reproduced by permission.

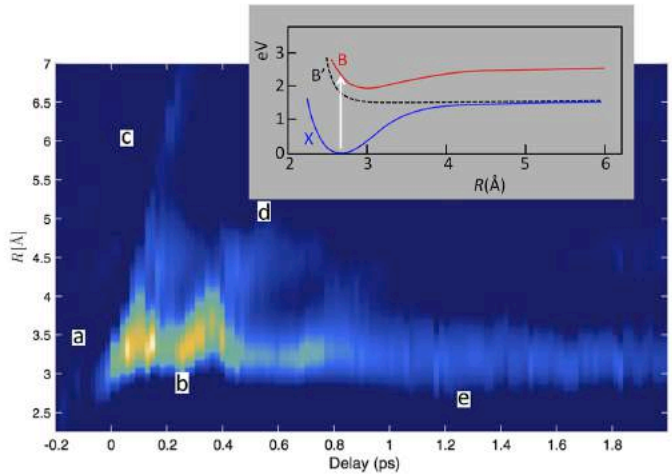

Fig. 46 – A recent result of the LCLS x-FEL [112], showing the evolution of iodine molecules after Frank-Condon optical transitions to excited electronic and vibrational states (upper-right inset). The cumulative data from many molecules show the interatomic distances as a function of time after the excitation. The phenomenon starts in region a, and region b shows the fingerprints of oscillations extending to the outer turning point (region d). But the results reveal other phenomena: molecular dissociation in region c, and rotational dephasing in region e [112]. Image from [122], copyright: American Physical Society, reproduced by permission.

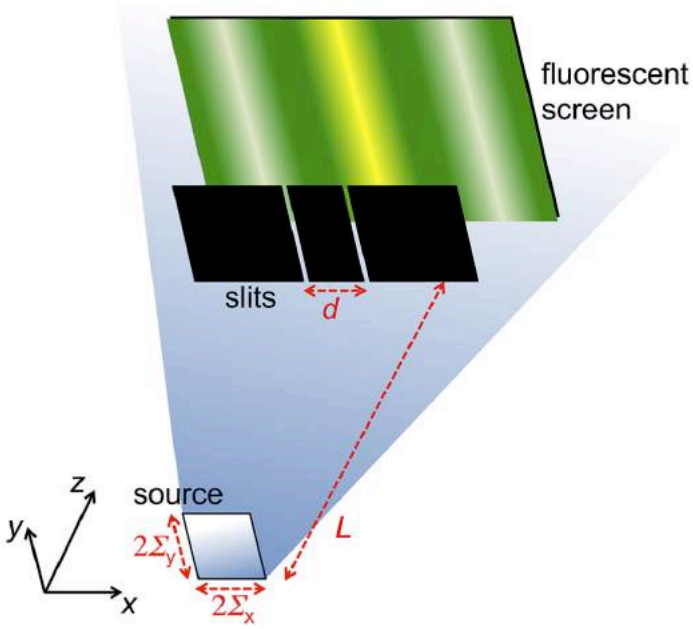

Fig. 47 – The simple two-slit experiment used to explain spatial and time coherence and the corresponding parameters.

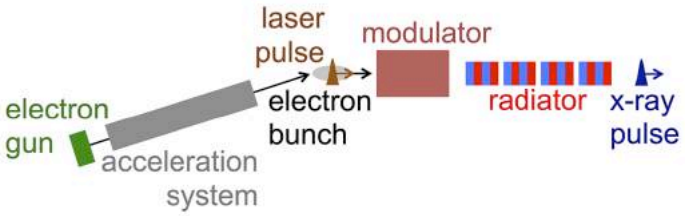

Fig. 48 – Simplified outline of a seeded x-FEL based on the HGHG mechanism [116]. A laser pulse and a relativistic electron bunch (produced by an electron gun and by an accelerator system) are injected together into the modulator section, where their interaction causes a periodic spatial modulation of the electron bunch. The modulator is designed to produce not only the fundamental modulation at the laser wavelength, but also strong higher harmonics. Then, the "radiator" system, including several undulators and other components, amplifies one of the higher harmonics. For a detailed description, see [116].

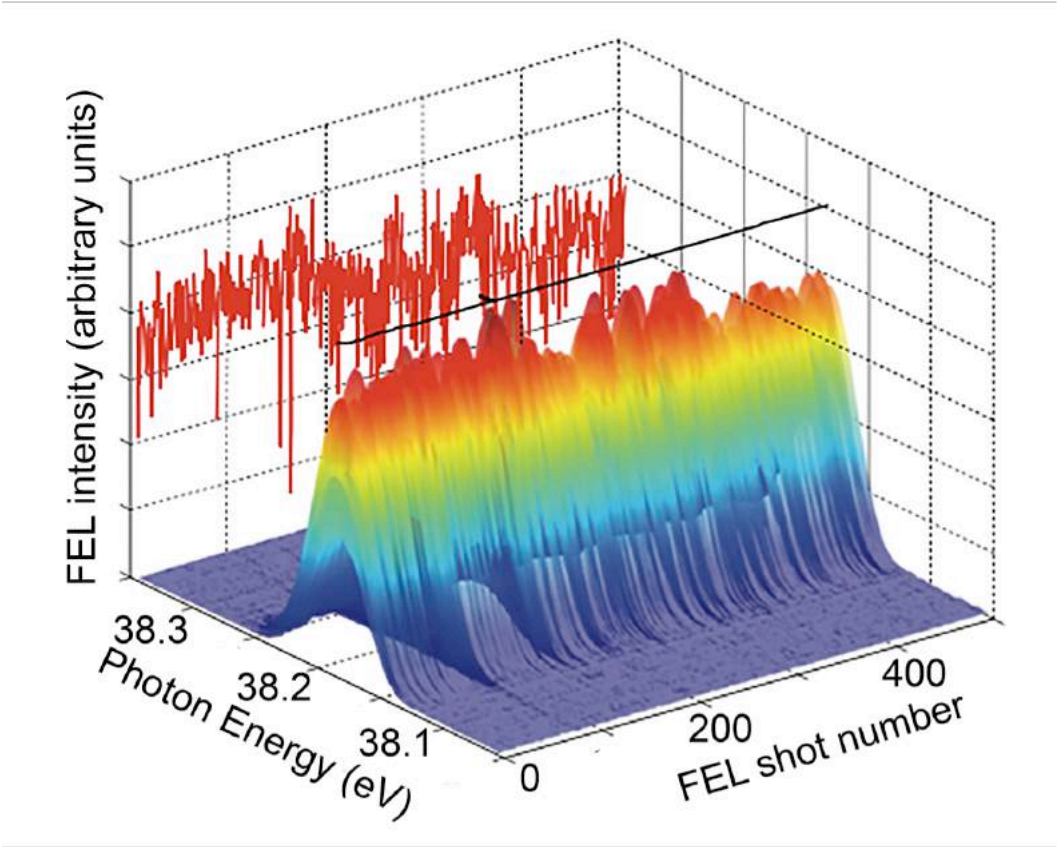

Fig. 49 – Results of HGHG seeding obtained in the FERMI x-FEL [116]. Note the excellent pulse-to-pulse stability, in contrast with the fluctuations of SASE x-FEL's [11]. Image from [116], copyright: Nature, reproduced by permission.